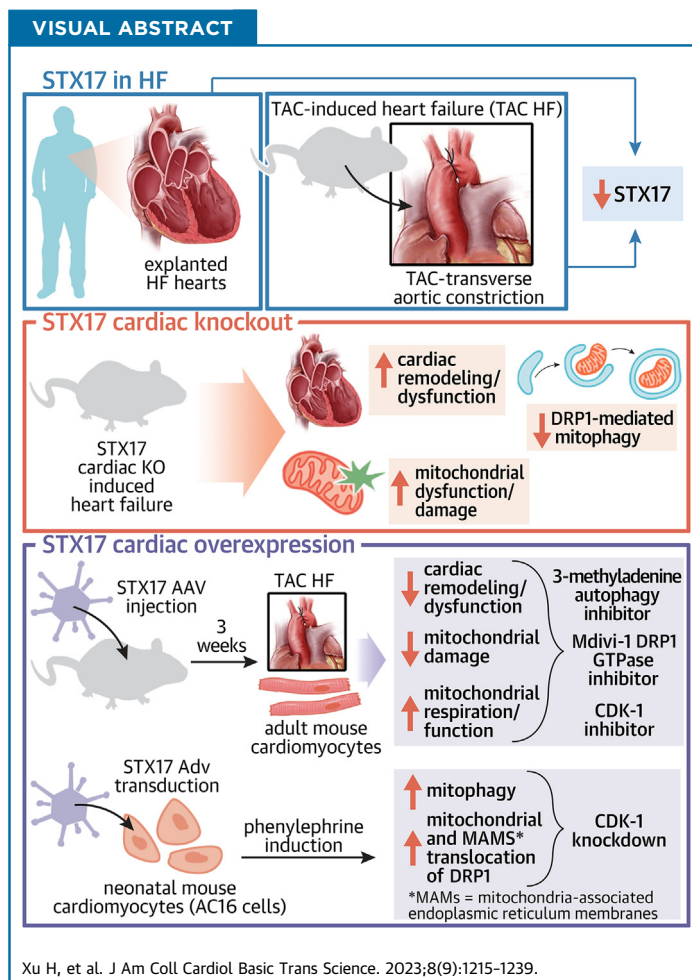


ORIGINAL RESEARCH - PRECLINICAL

# Syntaxin 17 Protects Against Heart Failure Through Recruitment of CDK1 to Promote DRP1-Dependent Mitophagy



Haixia Xu, MD,<sup>a,b</sup> Xiang Wang, MD,<sup>a</sup> Wenjun Yu, MD,<sup>a,c</sup> Shiqun Sun, MD,<sup>a</sup> Ne N. Wu, MD,<sup>a</sup> Junbo Ge, MD, PhD,<sup>a</sup> Jun Ren, MD, PhD,<sup>a,d</sup> Yingmei Zhang, MD, PhD<sup>a</sup>



**HIGHLIGHTS**

- STX17 level was significantly decreased in heart tissues from patients with HF and mice with TAC-induced HF.
- Cardiac specific STX17 knockout resulted in contractile dysfunction, mitochondrial damage, and insufficient mitophagy.
- STX17 overexpression attenuated TAC-induced left ventricular contractile dysfunction, mitochondrial damage, and mitophagy suppression.
- STX17 recruited CDK1 onto MAMs to phosphorylate DRP1 at Ser616 and promote DRP1-mediated mitophagy upon TAC or PE stress.

From the <sup>a</sup>Shanghai Institute of Cardiovascular Diseases, National Clinical Research Center for Interventional Medicine, Department of Cardiology, Zhongshan Hospital, Fudan University, Shanghai, China; <sup>b</sup>Department of Cardiology, Affiliated Hospital of Nantong University, Jiangsu, China; <sup>c</sup>Hubei Provincial Engineering Research Center of Minimally Invasive Cardiovascular Surgery, Department of Cardiovascular Surgery, Zhongnan Hospital of Wuhan University, Wuhan, China; and the <sup>d</sup>Department of Laboratory Medicine and Pathology, University of Washington, Seattle, Washington, USA.

## ABBREVIATIONS AND ACRONYMS

- AAV9** = adeno-associated virus serotype 9  
**CDK1** = cyclin-dependent kinase-1  
**CTNT** = cardiac troponin T  
**DRP1** = dynamin-related protein 1  
**HF** = heart failure  
**LC3** = light chain 3  
**MAM** = mitochondria-associated endoplasmic reticulum membrane  
**NC** = negative control  
**PE** = phenylephrine  
**STX17** = syntaxin 17  
**TAC** = transverse aortic constriction  
**TMRM** = tetramethylrhodamine methyl ester  
**3-MA** = 3-methyladenine

## SUMMARY

Mitochondrial dysfunction is suggested to be a major contributor for the progression of heart failure (HF). Here we examined the role of syntaxin 17 (STX17) in the progression of HF. Cardiac-specific *Stx17* knockout manifested cardiac dysfunction and mitochondrial damage, associated with reduced levels of p(S616)-dynamin-related protein 1 (DRP1) in mitochondria-associated endoplasmic reticulum membranes and dampened mitophagy. Cardiac STX17 overexpression promoted DRP1-dependent mitophagy and attenuated transverse aortic constriction-induced contractile and mitochondrial damage. Furthermore, STX17 recruited cyclin-dependent kinase-1 through its SNARE domain onto mitochondria-associated endoplasmic reticulum membranes, to phosphorylate DRP1 at Ser616 and promote DRP1-mediated mitophagy upon transverse aortic constriction stress. These findings indicate the potential therapeutic benefit of targeting STX17 in the mitigation of HF. (J Am Coll Cardiol Basic Trans Science 2023;8:1215-1239) © 2023 The Authors. Published by Elsevier on behalf of the American College of Cardiology Foundation. This is an open access article under the CC BY-NC-ND license (<http://creativecommons.org/licenses/by-nc-nd/4.0/>).

**H**ear failure (HF) is a complex and terminal pathophysiological stage of various cardiovascular diseases, representing a severe health care burden globally with a high morbidity, mortality, and hospitalization rate.<sup>1</sup> However, the molecular mechanisms only remain partially understood for HF, warranting identification of new therapeutic targets in the management of HF.

Mitochondria serve as the energy powerhouse in cardiomyocytes and account for approximately 30% of cardiomyocyte volume.<sup>2</sup> Emerging evidence has indicated a role for mitochondrial dysfunction as a major contributor to the progression of HF.<sup>3</sup> To sustain a network of functional mitochondria, cardiomyocytes employ a series of well-coordinated quality-control machineries, including mitochondrial biogenesis, mitochondrial fission and fusion, and mitophagy.<sup>4</sup> More recent evidence suggested an indispensable role for mitochondria-associated endoplasmic reticulum membranes (MAMs) in the governance of mitochondrial quality.<sup>5-7</sup> Mitochondria are coordinated with the sarcoplasmic/endoplasmic reticulum with 5% to 20% of mitochondrial membranes closely apposed (10-30 nm) to the sarcoplasmic/endoplasmic reticulum membranes, regulating a wide variety of physiological and pathophysiological processes including Ca<sup>2+</sup> communication, phospholipid exchange, mitochondrial biogenesis and dynamics, mitophagy, and cell death.<sup>8</sup>

Recent evidence has indicated that mitophagy is also under the fine-tuning of MAMs, governing the

clearance of long-lived and damaged mitochondria in physiological and pathophysiological settings.<sup>9,10</sup> For example, mitophagy was shown to serve as a compensatory and adaptive machinery to maintain mitochondrial integrity in murine hearts under transverse aortic constriction (TAC)-evoked pressure overload.<sup>11,12</sup> More evidence has indicated involvement of dynamin-related protein 1 (DRP1), a dynamin-related GTPase translocated onto the outer mitochondrial membrane to mediate mitochondrial fission, in mitophagy regulation.<sup>13-15</sup> Several independent reports have revealed existence of mitophagy abnormalities, onset of HF, and even lethality in conditional cardiac DRP1 knockout mice.<sup>11,16</sup> Furthermore, phosphorylation and mitochondrial outer membrane translocation of DRP1 were overtly upregulated 3 to 5 days following TAC surgery, the responses of which were temporally associated with changes in mitophagic flux.<sup>11</sup> Although these findings have shed some light toward a complex role of DRP1-dependent mitophagy in mitochondrial quality control,<sup>11,16</sup> further mechanistic study is still needed.

Syntaxin 17 (STX17), a SNARE scaffold protein localized on MAMs in addition to mitochondria and sarcoplasmic/endoplasmic reticulum, not only initiates the autophagy process, but also mediates the fusion of autophagosomes with lysosomes to form autophagolysosomes.<sup>17-20</sup> STX17 was reported to promote mitochondrial dynamics by interacting with DRP1 to regulate its localization and activity at MAMs.<sup>21,22</sup> However, whether STX17 coordinates with DRP1-dependent mitophagy and participates in the

The authors attest they are in compliance with human studies committees and animal welfare regulations of the authors' institutions and Food and Drug Administration guidelines, including patient consent where appropriate. For more information, visit the [Author Center](#).

progression of HF remain unclear. Herein, we aimed to evaluate the effect of STX17 genetic manipulation on cardiac and mitochondrial function in the face of pressure overload challenge, and possible mechanisms involved with a focus on DRP1-dependent mitophagy.

## METHODS

**HUMAN HEART SAMPLES AND EXPERIMENTAL ANIMAL MODELS.** Human heart samples were obtained from HF patients receiving heart transplants. Donor heart tissues not utilized for heart transplantation due to noncardiac causes were employed as nonfailing control tissues. Written informed consent was provided to the patients and family members of donors. The study was conducted in accordance with the Declaration of Helsinki and approved by the Institutional Ethics Committee of Sun Yat-Sen Memorial Hospital, Sun Yat-sen University, Guangzhou, China (SYSEC-KY-KS-2019-019).

Experimental animal procedures were approved by the Animal Care and Use Committee of Zhongshan Hospital Fudan University (Shanghai, China). All animal procedures were performed in accordance with the guidelines from Directive 2010/63/EU of the European Parliament on the protection of animals used for scientific purposes or the National Institutes of Health Guide for the Care and Use of Laboratory Animals. Cardiomyocyte *Stx17* conditional knockout (*Stx17<sup>cko</sup>*) mice were generated using *Stx17<sup>fl/fl</sup>* breeding with *Myh6-cre* transgenic mice (Gempharmatech Corporation). The exon3-exon4 of *Stx17-202* (ENSMUST00000107720.8) of the *Stx17* gene was chosen as the conditional knockout region, resulting in a frameshift of this gene. Littermates of genetically engineered mice (*Stx17<sup>fl/fl</sup>*) served as the flox control mice.

To achieve STX17 overexpression, male C57BL/6J mice (6 weeks) were intravenously injected with (tail vein) recombinant adeno-associated virus serotype 9 (AAV9) carrying Flag-STX17 with cardiac troponin T (cTNT) promoter (AAV9-cTNT-STX17) and negative control (NC) vectors (AAV9-cTNT-NC) at the dose of  $5 \times 10^{11}$  plaque-forming units (Obio Technology Corporation).

For the TAC procedure, adult male mice (8-10 weeks of age) were anesthetized using isoflurane (5% for induction and 1%-2% for maintenance) and were randomly subjected to TAC or sham surgery. Briefly, the transverse aorta was dissected at the aortic arch level free of surrounding tissues and a 6-0 nylon suture was tied around the aorta and a blunted

27-gauge needle to yield narrowing of luminal diameter. Then, the needle was removed following ligation. Mice in the sham group received identical procedures except the ligation. After 4 weeks following TAC or sham procedure, mice were sacrificed under isoflurane anesthesia/euthanasia (cervical dislocation) and hearts were harvested. A cohort of sham and TAC mice were administered 3-methyladenine (3-MA) (15 mg/kg, intraperitoneally injected) every 3 days to inhibit autophagic induction, or the cyclin-dependent kinase-1 (CDK1) inhibitor AZD5438 (50 mg/kg, intragastric, twice daily for 3 days), or an equal volume of normal saline. 3-MA (M9281; Sigma-Aldrich) and AZD5438 (MedChemExpress) were dissolved in dimethyl sulfoxide and then dilute with normal saline.

## GENE ONTOLOGY ANALYSIS AND VISUALIZATION.

Raw microarray data of GSE116250, including 14 nonfailing donors and 37 dilated cardiomyopathies, were downloaded from the Gene Expression Omnibus database. Genes with  $|\log\text{FoldChange}| > 0.36$  and a *P* value  $< 0.05$  were identified as differentially expressed genes.<sup>23</sup> Functional enrichment analysis of Gene Ontology was performed and visualized using the clusterProfiler package available in R software (version 4.1.1).<sup>24</sup>

**ECHOCARDIOGRAPHIC EVALUATION.** All mice were anesthetized with 2% isoflurane and were placed on a heating pad (37 °C) with a supine position. Heart rates were maintained at 450 to 600 beats/min for all mice. Cardiac geometry and function were evaluated using a Vevo 2100 M-mode echocardiography (VisualSonics). In brief, left ventricular dimensions including left ventricular end-diastolic diameter, left ventricular end-systolic diameter, left ventricular end-diastolic volume, and left ventricular end-systolic volume were recorded. Ejection fraction was calculated as (left ventricular end-diastolic volume - left ventricular end-systolic volume) / left ventricular end-diastolic volume, while fractional shortening was presented as (left ventricular end-diastolic diameter - left ventricular end-systolic diameter) / left ventricular end-diastolic diameter.

**HISTOLOGICAL ASSESSMENT.** Following deep anesthesia using isoflurane, mice were sacrificed by cervical dislocation and hearts were excised and placed in paraformaldehyde prior to the fixation in paraffin. Then, hearts were sliced into 5- $\mu\text{m}$ -thick sections. Cardiac fibrosis was evaluated using Masson trichrome staining. Cardiomyocyte cross-sectional area was estimated using wheat germ agglutinin (Sigma-Aldrich) staining. Images were captured using Leica

microscopy at  $\times 40$  objective (Leica) and were subsequently assessed using ImageJ software (Version 1.8; National Institutes of Health).<sup>25</sup>

An In-Situ Cell Death Detection Kit (Roche) was utilized to assess cardiomyocyte apoptosis.<sup>26</sup> Heart sections were incubated in a FITC-conjugated dUTP solution for 1 hour. Images were captured and the percentage of terminal deoxynucleotidyl transferase mediated dUTP nick end labeling-positive nuclei was calculated to evaluate myocardial apoptosis.

**TRANSMISSION ELECTRON MICROSCOPY.** Small blocks of heart samples were fixed with 2.5% glutaraldehyde and 0.1M sodium cacodylate (pH 7.4) at 4 °C. Thin sections were cut using an ultramicrotome and ultrastructural images were taken using a Hitachi H-7000 Electron Microscope. ImageJ software was employed to assess mitochondrial morphology. Fragmentation of mitochondrial cristae and irregular mitochondrial arrangement were deemed as damaged mitochondria. The ratio of damaged mitochondria to total mitochondria was evaluated.

**ISOLATION, CELL CULTURE, AND PHENYLEPHRINE CHALLENGE IN ADULT AND NEONATAL CARDIOMYOCYTES.** Adult mouse cardiomyocytes were isolated and cultured.<sup>27,28</sup> Adult male mice were anesthetized by isoflurane (5% for induction and 1%-2% for maintenance). Then, murine hearts were digested with collagenase II and IV (Worthington Biochem). Following gradual restoration of  $Ca^{2+}$  to physiological levels, rod-shaped Adult mouse cardiomyocytes were seeded onto confocal dishes or glass coverslips precoated with laminin (5  $\mu$ g/mL). The supernatants were collected to produce cardiac nonmyocyte fraction using centrifugation (300 g, 5 minutes) prior to culture in fibroblast growth media.

Neonatal mouse cardiomyocytes were isolated from hearts of 1-day-old C57BL/6J mice and were digested with collagenase I (Worthington Biochem). Cardiomyocytes were transduced with adenoviruses carrying LacZ, STX17, or shSTX17 at the indicated multiplicity of infection (= 20). Adenoviruses harboring short hairpin RNA for mouse STX17 (Ad-shSTX17) were generated using the following hairpin forming oligonucleotides: 5'-CCUAGAAGCGGACUUAAUTT-3'. Cohorts of cardiomyocytes were then treated with phosphate buffered saline (as control condition) or phenylephrine (PE) (100  $\mu$ M) for 48 hours.

**MITOCHONDRIAL FUNCTIONAL MEASUREMENT.** Mitochondrial membrane potential was examined using tetramethylrhodamine methyl ester (TMRM) (Invitrogen). Cardiomyocytes were incubated in a TMRM solution at 37 °C for 30 minutes. Mitochondrial

$O_2^-$  was measured using MitoSOX (Invitrogen). Cardiomyocytes were loaded with MitoSOX (1  $\mu$ M) for 10 minutes. Fluorescence intensity was captured using a laser confocal microscope (Leica).<sup>29</sup>

Adult mouse cardiomyocytes were seeded in a 96-well plate, and oxygen consumption rate was employed to detect mitochondrial adenosine triphosphate production and maximal respiration (xFe96 extracellular flux analyzer; Seahorse Biosciences).<sup>29</sup>

**AUTOPHAGY ASSESSMENT USING MT-KEIMA AND mRFP-GFP-LC3 ADENOVIRAL VECTOR.** Adult mouse cardiomyocytes or neonatal mouse cardiomyocytes were transduced with an mRFP-GFP-LC3 adenoviral vector (HanBio Technology). Briefly, isolated cardiomyocytes were cultured with adenoviruses at a final multiplicity of infection of 20 at 37 °C for 48 hours. Then, images were obtained using a Leica confocal microscope. Autophagic flux was evaluated by the number of yellow (early autophagosomes) and red (late autolysosomes) puncta.<sup>30</sup>

Next, autophagy was also evaluated using mt-keima (HanBio Technology), a pH-sensitive, lysosomal protease-resistant fluorescent probe, with its excitation wavelength shifting from 457 to 561 nm in an acidic environment of lysosomes. Cells were transfected with mt-keima adenoviruses (multiplicity of infection = 20) for 48 hours. Fluorescence captured under a laser confocal microscope (Leica) was analyzed using the ImageJ software.

**AC16 CELL CULTURE, PLASMIDS TRANSFECTION, AND SMALL INTERFERING RNA KNOCKDOWN.** HA-tagged DRP1, BFP-tagged CDK1, Flag-tagged CDK1, and His-tagged STX17 were cloned into pcDNA3.1(+) and generated in Genecefe Biotechnology Corporation. Human AC16 cardiomyocytes were cultured in Dulbecco's Modified Eagle Medium with 10% fetal bovine serum in a humidified incubator with 5%  $CO_2$  at 37 °C. Then, cells were transfected plasmids using the lipofectamine 3000 transfection reagent (Invitrogen) for 48 hours.

AC16 cells were transfected with a small interfering RNA negative control sample (scramble), small interfering RNA against CDK1 or STX17 for 48 hours (Genecefe Biotechnology Corporation). The small interfering RNA (1  $\mu$ g/ $\mu$ L) and lipofectamine 3000 transfection reagent were mixed together in an Opti-MEM medium (Thermo Fisher Scientific). Their sequences are presented as follows: 1) siSTX17, 5'-GCGAUACAGAAAUUCACUA TT-3'; 2) siSTX17, 5'-CCUAGAAGCGGACUUAAUTT-3'; 3) siSTX17, 5'-CCA-GAUCUCCUAGCCAAATT-3'; and 4) siCDK1, 5'-CCUAGUACUGCAAUUCGGGAAAUUU-3'.

For drug treatment, live cells were treated with mdivi-1 (10  $\mu$ M M0199, Sigma Aldrich) for 24 hours to inhibit DRP1 phosphorylation. Moreover, neonatal mouse cardiomyocytes were supplied with bafilomycin A1 (Baf A1, 50 nM; Sigma-Aldrich) for 4 hours to inhibit autophagy flux in the presence or absence of Ad-STX17 and PE for 48 hours.<sup>30</sup>

**MITOCHONDRIAL AND MAM PURIFICATION.** Mitochondria from heart tissues or cells were purified using a mitochondrial isolation kit (ab110168 or ab110170; Abcam). Heart tissues (30-50 mg) or cell lysates were suspended in an isolation buffer and Dounce homogenized. Then, pellets were centrifuged at 1,000 g for 10 minutes and supernatants were retained and centrifuged at 12,000 g for 15 minutes. After repeating these steps, the remaining pellets were resuspended using a RIPA buffer with a phosphatase/protease inhibitor.

MAM fractions were isolated according to the published procedures.<sup>31</sup> In brief, heart tissues or cells were Dounce homogenized with a mitochondrial isolation buffer and were centrifuged at 600 g for 5 minutes. Then, supernatant was recentrifuged at 7,000 g for 10 minutes to collect crude mitochondria (pellet), microsome, and endoplasmic reticulum fractions (supernatant). Then, crude mitochondrial fraction was centrifuged at 10,000 g for 10 minutes (Beckman). The crude mitochondrial pellet was resuspended in an isolation buffer prior to incubation in a Percoll medium. Following centrifugation at 95,000 g for 30 minutes, the MAM fraction was collected from the Percoll gradient and the pure mitochondria fraction was collected from the bottom of Percoll gradient. Then, MAM fraction was washed to remove Percoll using centrifugation at 6,300 g for 10 minutes. Supernatants were further centrifuged at 100,000 g for 1 hour to pellet the MAM fraction.

**CO-IMMUNOPRECIPITATION ANALYSIS.** Human AC16 cells overexpressing candidate proteins (HA-DRP1, His-STX17, Flag-CDK1) were harvested in a lysis buffer (50 mM Tris-HCl pH 7.5, 150 mM NaCl, 1% NP-40; Beyotime Biotechnology). After centrifugation at 12,000 rpm for 30 minutes, supernatants were immunoprecipitated with anti-HA, anti-His, or anti-Flag antibodies using Protein-A/G Agarose Beads (Invitrogen). Precipitants were examined using Western blot.

Proteomic analysis was performed by the liquid chromatography-tandem mass spectrometry (Bio-technology Corporation) as described.<sup>26</sup> Briefly, neonatal mouse cardiomyocytes were transduced with Ad-Flag-STX17 for 48 hours. Cells were then harvested and lysates were immunoprecipitated with the

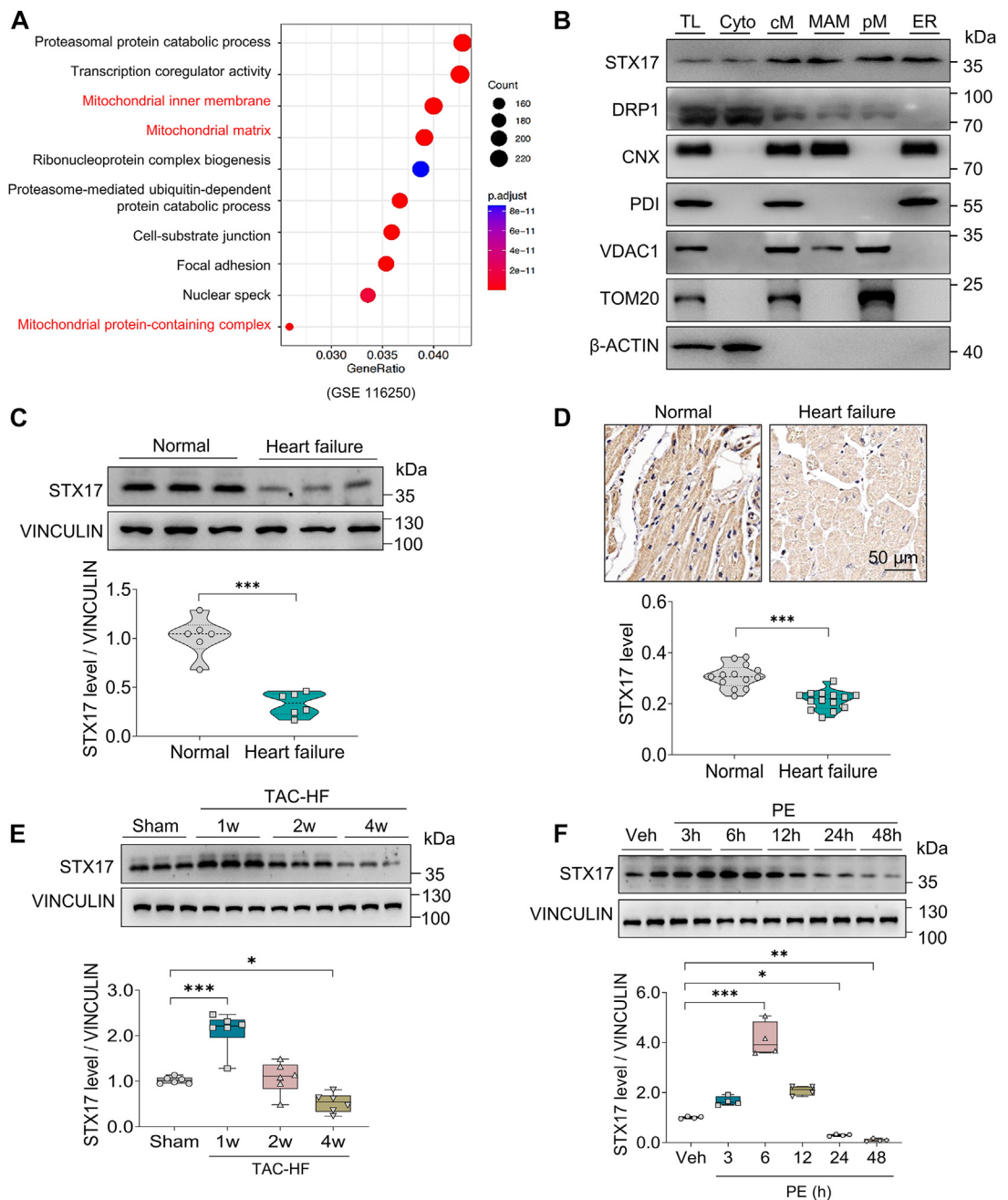
anti-Flag magnetic beads. Precipitates were examined using sodium dodecyl sulfate-polyacrylamide gel electrophoresis and were further digested for peptides extraction following by liquid chromatography-tandem mass spectrometry analysis.

**IMMUNOFLUORESCENCE CONFOCAL MICROSCOPY.** For immunofluorescence, cells were blocked and incubated with specified primary antibodies (Supplemental Table 1) overnight followed by respective Alexa Fluor secondary antibodies (1:500 dilution) at room temperature. Images were captured using a laser confocal microscope (Leica), and ImageJ software (Fiji) was used to quantitate colocalization between the 2 molecules.

**DUOLINK PROXIMITY LIGATION ASSAY ANALYSIS.** Duolink proximity ligation assay (Sigma-Aldrich) was employed to detect protein interaction (<40 nm) as an individual fluorescent dot using confocal microscopy according to the manufacturer's protocol. Myocardium sections or cells were permeabilized in phosphate-buffered saline containing 0.3% Triton X-100 for 30 minutes and were blocked for 1 hour. Thereafter, cells were incubated with corresponding mouse-plus and rabbit-minus probes for 1 hour in the dark. Immunofluorescence was detected on a laser confocal microscope (Leica).

**STRUCTURE-BASED PROTEIN INTERACTION INTERFACE PREDICTION.** The protein structure of STX17 was predicted with SWISS-MODEL tool (Swiss Institute of Bioinformatics, University of Basel), using PDB structure 3C98, chain B (covering residues 25-218) as the template. The protein structure of CDK1 was predicted using PDB structure 4Y72, chain A (covering residues 1-297, sequence identity = 100%) as the template. Structures of both STX17 and CDK1 were submitted to the PRISM tool (Swiss Institute of Bioinformatics, University of Basel) to analyze their potential interaction interface. Then, the prediction results were visualized using the PyMol tool (Swiss Institute of Bioinformatics, University of Basel).<sup>32</sup>

**REAL-TIME POLYMERASE CHAIN REACTION.** Total RNA of heart tissues was extracted and then reverse transcribed. Real-time polymerase chain reaction was performed according to the previous study.<sup>25</sup> All the primers are shown as follows: atrial natriuretic peptide (forward primer: 5'-TGCACACTTGGAGTGCCATTA-3'; reverse primer: 5'-TGTTTCAGGCA TAGGAGACCATAA-3'); B-type natriuretic peptide (forward primer: 5'-TGCACACTTGGAGTGCCATTA-3'; reverse primer: 5'-TGTTTCAGGCATAGGAGACCATAA-3');  $\beta$ -myosin heavy chain (forward primer: 5'-TGCACACTTGGAGTGCCATTA-3'; reverse primer: 5'-TGTTTCAGGCATAGGAGACCATAA-3'); mitochondrial DNA content was

**FIGURE 1 STX17 Levels Are Decreased in the Hearts of Patients With HF and Mice With TAC-Induced HF**

(A) Bubble plot exhibiting top 10 enrichment of Gene Ontology analysis (including cellular component, biological processes and molecular function) for transcripts in hearts from 14 nonfailing donors and 37 dilated cardiomyopathy patients (GSE116250). (B) Representative immunoblots of syntaxin 17 (STX17), dynamin-related protein 1 (DRP1), calnexin (CNX), protein disulfide isomerase (PDI), voltage-dependent anion channel 1 (VDAC1), translocase of the outer membrane 20 (TOM20) and β-actin in total lysates (TL), cytosol (cyto), crude mitochondria (cM), mitochondria-associated endoplasmic reticulum membranes (MAMs), pure mitochondria (pM), and endoplasmic reticulum fractions of murine heart tissues. (C) Western blot analysis of STX17 in myocardial tissues from normal or heart failure (HF) patients,  $n = 6$ . (D) Representative and quantitative immunohistochemical analysis of STX17 in myocardial tissues from normal or HF patients. Scale bar = 50 μm,  $n = 15$  fields per group. (E) Western blot analysis of STX17 in mouse hearts at different time points following transverse aortic constriction (TAC) surgery,  $n = 6$ . (F) Western blot analysis of STX17 in adult mouse cardiomyocyte at different time points following PE (phenylephrine) treatment,  $n = 4$ . Data are shown as mean ± SEM. Two-group comparison was performed using Student's  $t$  test (2-tailed), and data of different time points were compared with a repeated-measures 1-way analysis of variance test. \* $P < 0.05$ , \*\* $P < 0.01$ , and \*\*\* $P < 0.001$ .

detected using polymerase chain reaction with the gene sequences encoding mitochondrial cytochrome c oxidase 1 (*mtCOI*) as primers (forward primer: 5'-GCCCCGATATGGCGTTT-3'; reverse primer: 5'-GTTCACCTGTTCTCTGCTCC-3');  $\beta$ -actin (forward primer: 5'-TGCACACTTGAGTGCCATTA-3'; reverse primer: 5'-TGTTTCAGGCATAGGAGACCATAA-3').

**WESTERN BLOT.** Equal amounts of samples were subjected to 10% to 12% sodium dodecyl sulfate-polyacrylamide gel electrophoresis and were then transferred to polyvinylidene fluoride membranes (Merck Millipore). Following a 1-hour block, polyvinylidene fluoride membranes were incubated with respective primary antibodies (Supplemental Table 1) at 4 °C overnight. Blots were rinsed in Tris-buffered saline with Tween20 for 3 times prior to incubation with an horseradish peroxidase-conjugated secondary antibody for 1 hour at room temperature. Immunoblot gel density was detected using an enhanced chemiluminescence reagent and film was scanned and intensity of immunoblot bands was quantitated using a Bio-Rad Calibrated Densitometer. The gray value was analyzed with Image Lab 3.0 software (National Institutes of Health).

**STATISTICAL ANALYSIS.** Data are expressed as the mean  $\pm$  SEM. All statistical analyses were performed using GraphPad Prism 8.0 software (GraphPad Software). Two groups were compared using Student's *t* test, while multiple groups were compared using a repeated-measures 1-way analysis of variance test or 1-way analysis of variance followed by Tukey's post hoc test for multiple pairwise comparisons. The cumulative survival time was calculated by the Kaplan-Meier method and the log-rank test was applied to compare between 2 groups. A 2-sided *P* value <0.05 was considered statistically significant.

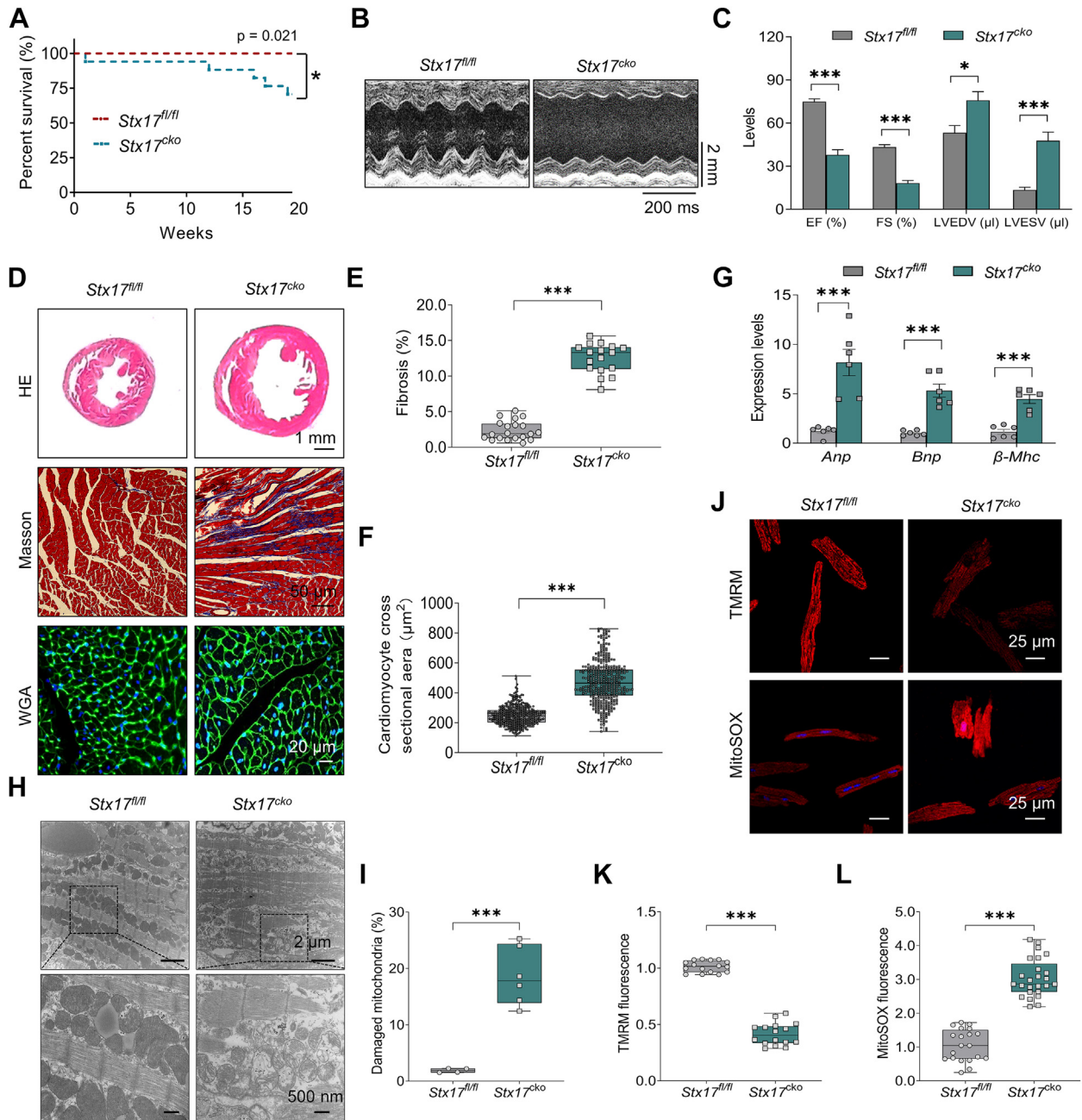
## RESULTS

**STX17 LEVELS WERE DOWNREGULATED IN THE HEART TISSUES OF PATIENTS WITH HF AND MICE WITH TAC-INDUCED HF.** To explore the underlying mechanism in HF, the Gene Expression Omnibus database was searched and microarray dataset GSE116250 was downloaded. Gene Ontology analysis showed that differentially expressed genes between control and TAC-induced HF mouse hearts were mainly enriched in "Mitochondrial inner membrane," "Mitochondrial matrix," and "Mitochondrial protein-containing complex" (Figure 1A), indicating an important role of mitochondrial homeostasis in the progression of HF. STX17, as a conserved molecule on the mitochondrial membranes, endoplasmic reticulum

membrane, and MAMs, was reported to regulate mitochondrial homeostasis. Our data also depicted the presence of STX17 in the microsomal, mitochondrial, and MAM fractions (Figure 1B). Immunofluorescence data also uncovered the presence of STX17 not only in the mitochondria, but also in the sarcoplasmic reticulum in cardiomyocytes (Supplemental Figure 1).

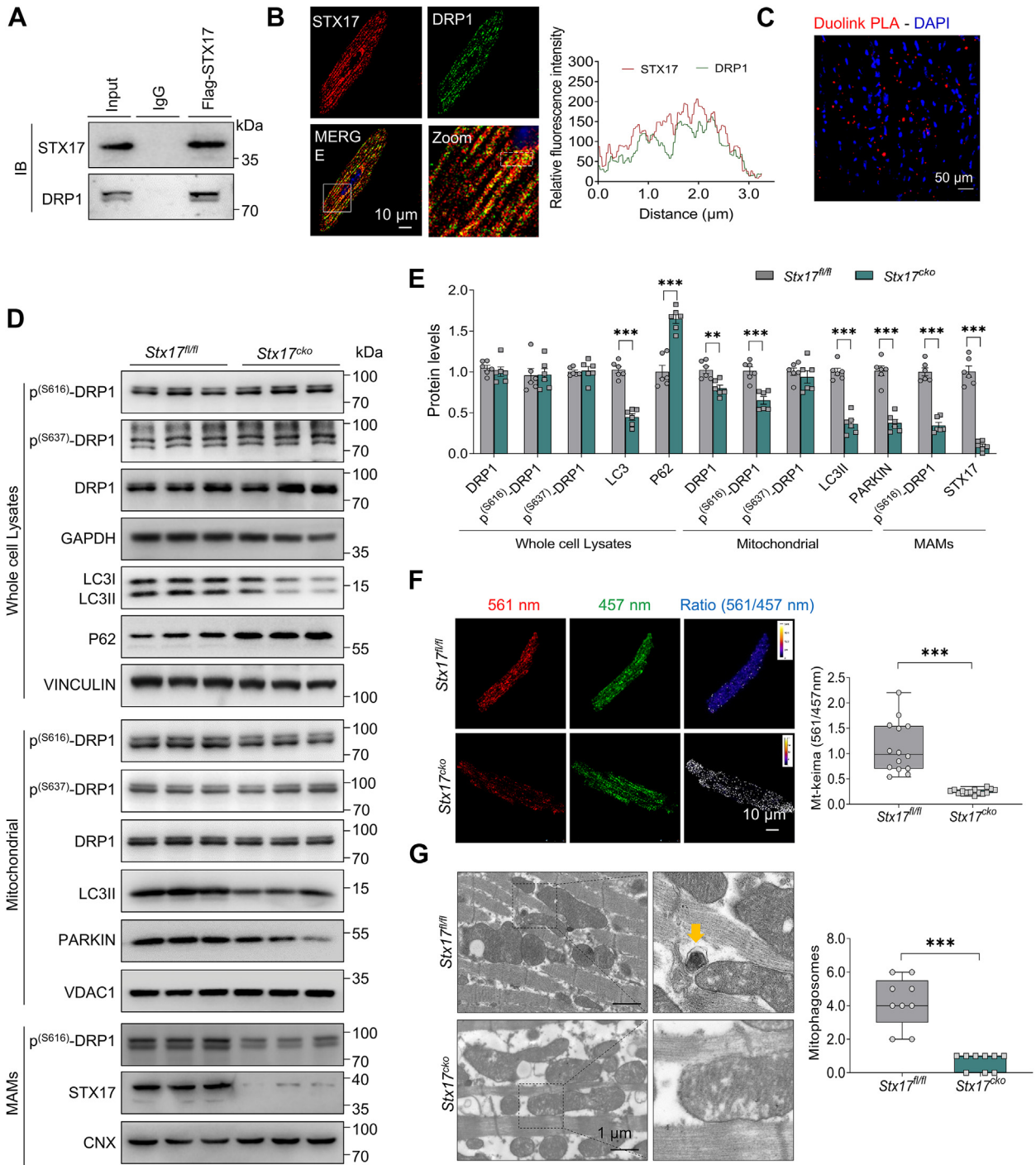
To discern the possible role of STX17 in HF, levels of STX17 were detected in heart tissues from patients with HF. Our data showed that STX17 protein levels were reduced in hearts of HF patients compared with nonfailing myocardium (Figure 1C). A similar reduction of STX17 levels was noted using immunohistochemical analysis (Figure 1D). Next, STX17 levels in the hearts of mice after TAC surgery at 1, 2, and 4 weeks were estimated. Our data revealed that STX17 levels were transiently increased at 1 week following TAC, but they were gradually declined at 2 and 4 weeks after TAC in murine hearts (Figure 1E). Adult mouse cardiomyocytes were isolated and treated with PE stimulation for up to 48 hours. Results shown in Figure 1F revealed that STX17 levels were transiently increased at 3 and 6 hours in the face of PE challenge, although they were gradually declined at 12, 24, and 48 hours following PE treatment. To decipher the source of declined STX17 for the downregulation of myocardial STX17 in HF, cardiomyocytes or cardiac nonmyocytes were isolated from sham and TAC-induced HF mice. Our data revealed that STX17 levels were significantly decreased in cardiomyocytes of TAC-induced HF but not in nonmyocytes (Supplemental Figures 2A and 2B).

**CARDIAC STX17 KNOCKOUT RESULTED IN CARDIAC DYSFUNCTION AND MITOCHONDRIAL DAMAGE.** To explore the role of STX17 in cardiac dysfunction, mice with cardiac-specific *Stx17* knockout were generated using homozygous flox *Stx17* alleles (*Stx17<sup>fl/fl</sup>*) with standard *Myh6*-Cre mice to induce late embryonic/early postnatal cardiomyocyte-specific *Stx17* gene deletion (Supplemental Figure 3A). This strategy dramatically reduced cardiac STX17 protein levels (Supplemental Figures 3B to 3D) for assessment of endogenous STX17 on cardiac function. Analysis of embryonic sections indicated no cardiac dysplasia of myocardium at E14 compared with wild-type embryos (Supplemental Figure 4A). Although cardiac *Stx17* knockout did not lead to embryonic lethality, these mice displayed a higher mortality (Figure 2A). Cardiac structural and functional analyses showed that STX17 deletion resulted in overt contractile dysfunction compared with *Stx17<sup>fl/fl</sup>* littermates or *Myh6*-cre transgenic mice. Our data showed that cardiac *Stx17* knockout significantly decreased ejection

**FIGURE 2** Cardiac *Stx17* Knockout Resulted in Contractile Dysfunction and Mitochondrial Damage

Cardiac-specific *Stx17* knockout (*Stx17<sup>fl/fl</sup>Myh6<sup>Cre</sup>*, *Stx17<sup>cko</sup>*) mice were generated. Littermates (*Stx17<sup>fl/fl</sup>*) were considered as flox control mice. **(A)** The survival curve of *Stx17<sup>fl/fl</sup>* and *Stx17<sup>cko</sup>* mice,  $P = 0.021$  (log-rank test). **(B, C)** Representative echocardiographic images and quantitative data in *Stx17<sup>cko</sup>* and *Stx17<sup>fl/fl</sup>* mice (12 weeks) including ejection fraction (EF), fractional shortening (FS), left ventricular end-diastolic volume (LVEDV), and left ventricular end-systolic volume (LVESV). **(D)** Representative heart slices using hematoxylin and eosin (scale bar = 1 mm), Masson trichrome (scale bar = 50  $\mu$ m), and wheat germ agglutinin (WGA) (scale bar = 20  $\mu$ m) staining in *Stx17<sup>cko</sup>* and *Stx17<sup>fl/fl</sup>* mice. **(E)** Quantitative analysis of cardiac fibrosis using Masson trichrome staining,  $n = 15$  to 20 fields per group. **(F)** Quantitative analysis of cross-sectional area of cardiomyocytes using WGA staining,  $n = 4$  to 6 mice per group. **(G)** Quantitative data of messenger RNA levels of atrial natriuretic peptide (*Anp*), B-type natriuretic peptide (*Bnp*), and  $\beta$ -myosin heavy chain ( $\beta$ -*Mhc*),  $n = 6$  mice per group. **(H, I)** Transmission electron microscopy images and quantitative analysis of mitochondrial morphology. Scale bars = 2  $\mu$ m or 500 nm,  $n = 4$  to 6 mice per group. **(J, L)** Representative and quantitative analysis of adult mouse cardiomyocytes isolated from *Stx17<sup>cko</sup>* and *Stx17<sup>fl/fl</sup>* mice stained with tetramethylrhodamine methyl ester (TMRM) to detect mitochondrial membrane potential and MitoSOX to detect mitochondrial reactive oxygen species generation. Scale bar = 25  $\mu$ m,  $n = 16$  to 20 fields per group. Data are shown as mean  $\pm$  SEM. Two-group comparison was performed using Student's *t* test (2-tailed). \* $P < 0.05$  and \*\*\* $P < 0.001$  vs the *Stx17<sup>fl/fl</sup>* group. Abbreviations as in Figure 1.

**FIGURE 3** Cardiac *Stx17* Knockout Inhibited p(S616)-DRP1 Levels in MAMs and Resulted in the Mitophagy Insufficiency



Continued on the next page

fraction and fractional shortening, along with remarkably increased left ventricular end-diastolic volume and left ventricular end-systolic volume (Figures 2B and 2C, Supplemental Figures 4B and 4C). Results shown in Figures 2D to 2F and Supplemental Figures 4D to 4F also revealed that *Stx17* knockout resulted in pathological heart enlargement, cardiac fibrosis, and increased cross-sectional area of cardiomyocytes. Moreover, cardiac STX17 deletion overtly increased messenger RNA levels of HF markers, including atrial natriuretic peptide, B-type natriuretic peptide, and  $\beta$ -myosin heavy chain compared with *Stx17<sup>fl/fl</sup>* littermates (Figure 2G).

Given the presence of STX17 in mitochondrial membrane and MAMs, to discern whether mitochondrial function was associated with STX17 deletion in failing hearts, mitochondrial abnormalities including ultrastructure of mitochondria, mitochondrial membrane potential, and mitochondrial reactive oxygen species production were detected. Mitochondrial architectural aberrations such as fragmentation of mitochondrial cristae, irregular mitochondrial arrangement, and mitochondrial swelling were observed in *Stx17<sup>cko</sup>* mouse myocardium using transmission electron microscopy (Figures 2H and 2I). Cardiac *Stx17* knockout overtly increased damaged mitochondria, suggesting mitochondrial dysfunction in *Stx17<sup>cko</sup>* hearts. Next, TMRM and MitoSOX were assessed in adult mouse cardiomyocytes isolated from *Stx17<sup>cko</sup>* and *Stx17<sup>fl/fl</sup>* mice. Results shown in Figures 2J to 2L and Supplemental Figures 4G to 4I revealed that STX17 deletion collapsed mitochondrial membrane potential and provoked mitochondrial reactive oxygen species accumulation.

**CARDIAC STX17 KNOCKOUT INHIBITED p(S616)-DRP1 LEVELS IN MAMs AND EVOKED MITOPHAGY INSUFFICIENCY.** STX17 was found to regulate mitochondrial dynamics and homeostasis through interaction with DRP1, rather than through other mitochondrial fusion and fission molecules in HeLa and 293T cells.<sup>22</sup> Furthermore, DRP1-mediated

mitochondrial quality control plays a critical role in cardiomyocytes.<sup>16</sup> Our results also noted that levels of p(S616)-DRP1 were transiently upregulated before a gradual decline at 2 and 4 weeks following TAC in mitochondrial fractions, coinciding with tendency of STX17 in murine hearts following TAC challenge (Supplemental Figure 5). To discern the potential effect of DRP1-mediated mitochondrial quality control in STX17-deficient cardiomyocytes, interaction of STX17 with DRP1 was evaluated in neonatal mouse cardiomyocytes. Indeed, coimmunoprecipitation experiments demonstrated that Flag-STX17 interacted with DRP1 (Figure 3A). Concomitantly, immunofluorescence colocalization analysis in adult mouse cardiomyocytes and Duolink proximity ligation assay data in myocardium also verified the interaction of STX17 with DRP1 (Figures 3B and 3C). Then, levels of DRP1, p(S616)-DRP1, and p(S637)-DRP1 were evaluated. Our data failed to detect apparent changes of total DRP1, p(S616)-DRP1, and p(S637)-DRP1 levels in whole-cell lysates between *Stx17<sup>cko</sup>* and *Stx17<sup>fl/fl</sup>* murine hearts. However, a modest drop in p(S616)-DRP1 [but not p(S637)-DRP1] in the mitochondrial fractions and a robust reduction of pan and p(S616)-DRP1 in the MAM fractions were observed. A significant reduction in light chain 3I (LC3I) and LC3II levels in conjunction with elevated P62 levels were noted in whole-cell lysates of *Stx17<sup>cko</sup>* hearts in comparison with *Stx17<sup>fl/fl</sup>* mice. Similar remarkable decreases of LC3II and PARKIN levels were revealed in mitochondrial fractions, whereas no discernible change was observed in the distribution of p(S637)-DRP1 in mitochondrial fractions or levels of calnexin in MAM fractions (Figures 3D and 3E). Adult mouse cardiomyocytes from *Stx17<sup>cko</sup>* and *Stx17<sup>fl/fl</sup>* mice were transfected with mt-Keima adenovirus to evaluate mitophagic flux. Our data revealed that mitophagy activity, determined using mt-Keima ratio (561/457 nm) and autophagosomes containing mitochondria, was remarkably downregulated in STX17-deleted cardiomyocytes (Figures 3F and 3G). Moreover, relative

#### FIGURE 3 Continued

(A) Representative immunoprecipitation blots (IBs) with an anti-Flag or an anti-DRP1 antibody in neonatal mouse cardiomyocyte transduced with Ad-Flag-STX17 for 48 hours. (B) Representative immunofluorescence images and plot profile analysis of STX17 and DRP1. Scale bar = 10  $\mu$ m. Adult mouse cardiomyocytes were transduced with an Ad-Flag-STX17 adenovirus at the multiplicity of infection of 20 for 24 hours. (C) Representative Duolink proximity ligation assay (PLA) analysis of STX17 and DRP1 in the myocardium of control mice. (D, E) Representative immunoblots and quantitative data of DRP1, p(S616)-DRP1, p(S637)-DRP1, GAPDH (loading control), LC3, P62, and VINCULIN (loading control) in the whole-cell lysates DRP1, p(S616)-DRP1, p(S637)-DRP1, PARKIN, light chain 3II (LC3II), and VDCA1 (loading control) in the mitochondrial fractions; and p(S616)-DRP1, STX17, and CNX (loading control) in the MAM fractions in the heart tissues of *Stx17<sup>cko</sup>* and *Stx17<sup>fl/fl</sup>* mice, n = 6. (F) Representative confocal microscopic images and quantitative data of mt-keima, as adult mouse cardiomyocytes isolated from *Stx17<sup>cko</sup>* and *Stx17<sup>fl/fl</sup>* mice were transduced with the mt-keima adenovirus (multiplicity of infection = 20) for 48 hours. Scale bar = 10  $\mu$ m, n = 16 fields per group. (G) Representative transmission electron microscopy images and quantitative analysis of mitophagosomes, n = 9 fields per group. Data are shown as mean  $\pm$  SEM. Two-group comparison was performed using Student's t test (2-tailed). \*\*P < 0.01 and \*\*\*P < 0.001 vs the *Stx17<sup>fl/fl</sup>* group. Ig = immunoglobulin; other abbreviations as in Figure 1.

mitochondrial DNA contents were also significantly accumulated in *Stx17<sup>cko</sup>* hearts (Supplemental Figure 4J). These results indicated that STX17 deletion inhibited MAMs translocation of p(S616)-DRP1 and mitophagy activity, subsequently suppressing autophagic clearance of damaged mitochondria.

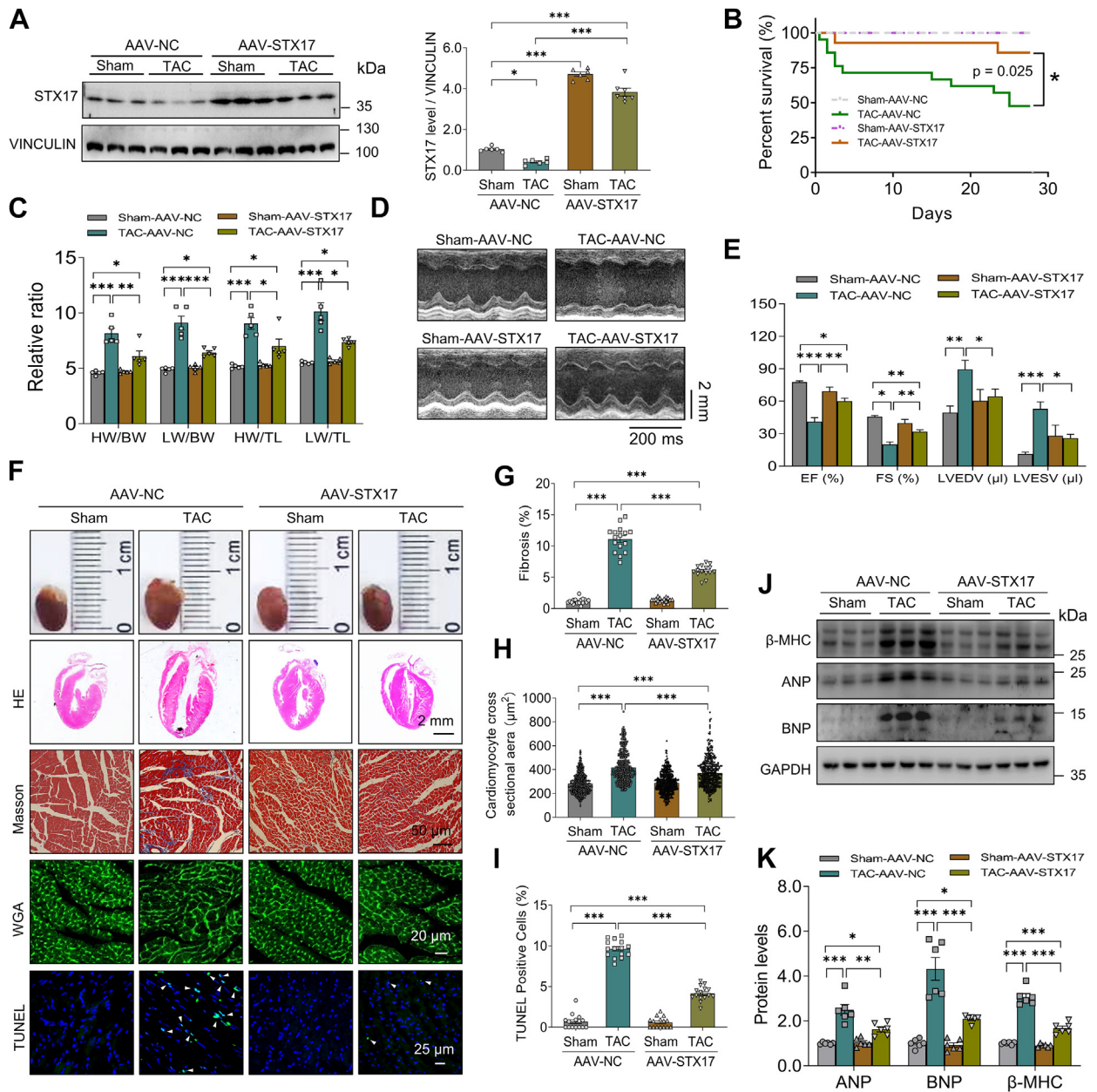
**STX17 OVEREXPRESSION ATTENUATED TAC-INDUCED HF AND CARDIAC REMODELING.** To further demonstrate the effect of STX17 in HF, AAV-cTNT-STX17 or negative control (AAV-NC) was injected to mice via tail veins 3 weeks prior to TAC surgery. STX17 viral transduction was validated using Western blot and immunofluorescence in myocardium (Figure 4A, Supplemental Figure 6A). Mouse survival rate was remarkably decreased following TAC surgery, the effect of which was reversed by STX17 overexpression (Figure 4B). Four weeks following TAC surgery, heart weight normalized to body weight, lung weight normalized to body weight, heart weight normalized to tibial length, and lung weight normalized to tibial length were remarkably increased in TAC mice compared with sham-operated mice, the effect of which was partially reversed by STX17 overexpression (Figure 4C). Echocardiographic and morphological properties were evaluated in AAV-NC and AAV-STX17 mice with or without the TAC procedure. Our results showed that the TAC procedure significantly increased left ventricular end-diastolic volume and left ventricular end-systolic volume as well as reduced ejection fraction and fractional shortening, the effects of which were partially alleviated by cardiac STX17 overexpression with little effect from STX17 overexpression itself (Figures 4D and 4E). Gross morphologies showed pathological heart enlargement in TAC mice, the effect of which was mitigated by STX17 overexpression (Figure 4F). Furthermore, STX17 overexpression protected against TAC-induced cardiac fibrosis (Figures 4F and 4G). Analysis of cardiomyocyte cross-sectional area and apoptosis revealed remarked increases in both parameters following TAC, the effects of which were partially reversed by STX17 overexpression (Figures 4H and 4I, Supplemental Figures 7A and 7B). Moreover, TAC overtly increased protein levels of HF markers including atrial natriuretic peptide, B-type natriuretic peptide, and  $\beta$ -myosin heavy chain, with the effect partially restored in STX17 overexpression mice (Figures 4J and 4K). STX17 overexpression itself did not exert any effect on cardiac geometric properties and markers for heart failure.

**CARDIAC STX17 OVEREXPRESSION ALLEVIATED TAC-INDUCED MITOCHONDRIAL DAMAGE IN CARDIOMYOCYTES.** Furthermore, mitochondrial

function was evaluated in adult mouse cardiomyocytes isolated from mice with cardiac STX17 overexpression underwent TAC-induced HF. TMRM and MitoSOX data revealed that TAC decreased mitochondrial membrane potential and increased mitochondrial reactive oxygen species generation, the effects of which were attenuated by STX17 overexpression with little influence from the viral vector itself (Figures 5A and 5B). Levels of mitochondrial respiratory electron transport chain complex including complex I, II, III, IV, and V were evaluated using Western blot. Results showed that TAC surgery downregulated levels of respiratory chain components including complex II, IV, and V, the effect of which was rescued by STX17 overexpression (Figure 5C). Then, transmission electron microscopy was used to evaluate the ultrastructure of mitochondria. Results showed irregular mitochondrial arrangement and disorganized, swollen, or reduced density mitochondrial cristae in myocardium with TAC-induced HF. Proportion of damaged mitochondria was much higher within TAC-induced HF, the effect alleviated by STX17 overexpression. STX17 overexpression alone exerted little discernable responses on mitochondrial morphology (Figures 5D and 5E). In addition, assessment of oxygen consumption rate showed that maximal respiration and adenosine triphosphate production were both significantly suppressed in adult mouse cardiomyocytes from TAC-challenged mice, the effects of which were partially improved by STX17 overexpression (Figures 5F to 5H). These data suggested that STX17 overexpression alleviated TAC-induced mitochondrial anomalies in cardiomyocytes.

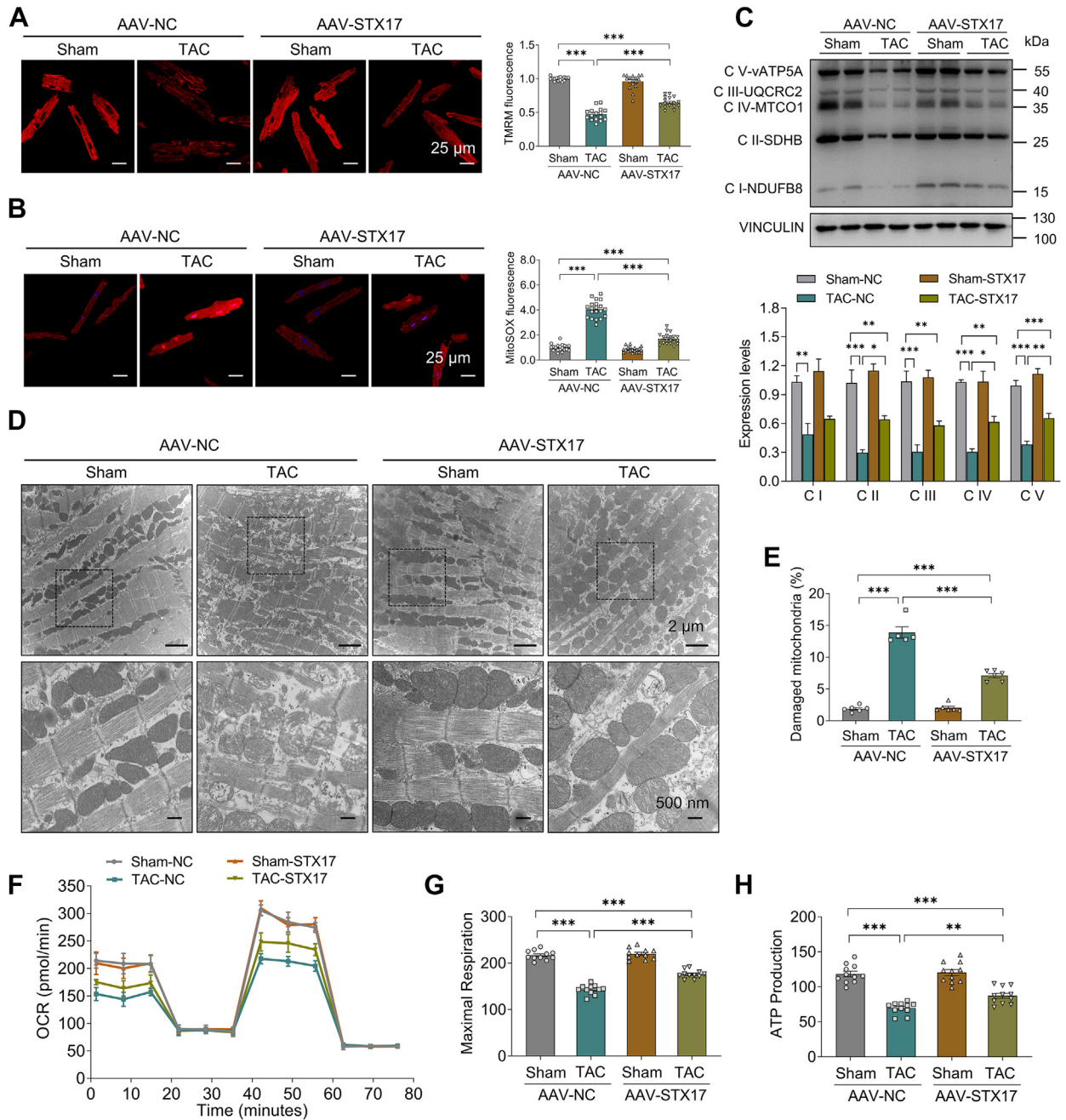
**STX17 OVEREXPRESSION IMPROVED MITOCHONDRIAL FUNCTION VIA DRP1-DEPENDENT MITOPHAGY.** To understand if cardiac protection of STX17 on TAC-induced HF is associated with DRP1-dependent mitophagy, expression of DRP1 and p(S616)-DRP1 in subcellular fractions was evaluated. Our data failed to note any overt change of DRP1 and p(S616)-DRP1 in whole-cell lysates of STX17 overexpressed myocardium in the presence or absence of TAC challenge. However, the TAC procedure induced a mild downregulation of p(S616)-DRP1 in mitochondrial fractions and a robust reduction of p(S616)-DRP1 in MAM fractions, the effects of which were partially reversed by STX17 overexpression. STX17 overexpression alone failed to affect p(S616)-DRP1 levels under normal conditions. In line with these results, downregulated LC3II and upregulated P62 levels in whole-cell lysates along with remarkably reduced LC3II levels in mitochondrial fractions of heart tissues were

**FIGURE 4 STX17 Overexpression Attenuated TAC-Induced Ventricular Dysfunction and Cardiac Remodeling**



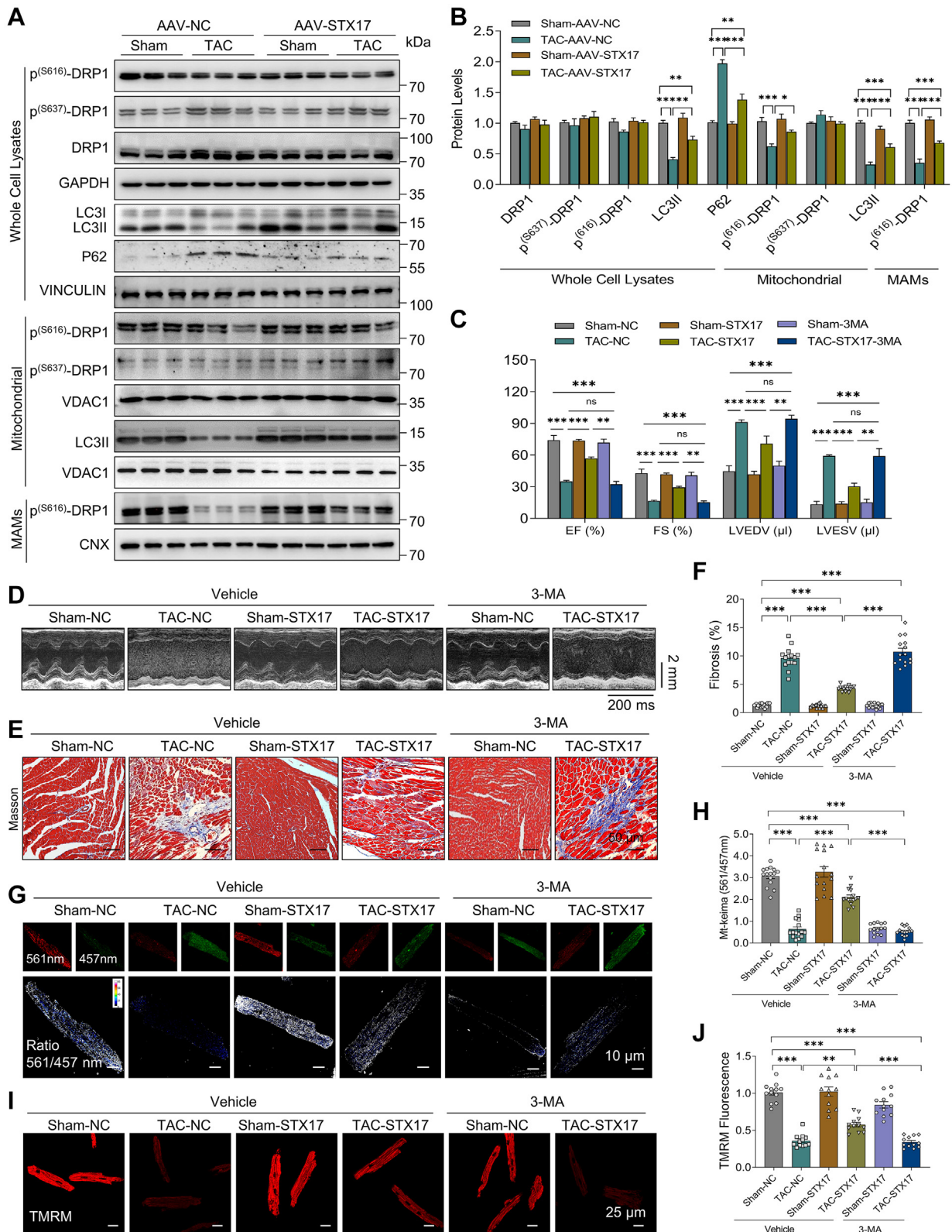
Male C57BL/6J mice were intravenously injected with an adeno-associated virus serotype 9 (AAV)-carrying Flag-tagged STX17 (AAV-STX17) with cardiac troponin T promoter at the dose of  $5 \times 10^{11}$  plaque-forming units and were randomly assigned to a sham group or TAC group for 4 weeks. **(A)** Representative immunoblots and quantitative data of STX17 levels and VINCULIN (loading control) in murine cardiac tissues,  $n = 6$  mice per group. **(B)** Survival curve of mice following TAC procedure in the presence or absence of STX17 overexpression,  $P = 0.025$  (TAC-STX17 group [ $n = 15$ ] vs TAC-NC group [ $n = 20$ ]) (log-rank test). **(C)** Quantitative data of heart weight normalized to body weight (HW/BW), lung weight normalized to body weight (LW/BW), heart weight normalized to tibia length (HW/TL), and lung weight normalized to tibia length (LW/TL),  $n = 4$  to 6 mice per group. **(D, E)** Representative echocardiographic images and quantitative data including EF, FS, LVEDV, and LVESV,  $n = 4$ -6 mice per group. **(F)** Representative cardiac morphology and heart slices using H&E (scale bar = 2 mm), Masson trichrome (scale bar = 50  $\mu$ m), and WGA (scale bar = 20  $\mu$ m) staining and terminal deoxynucleotidyl transferase mediated dUTP nick end labeling (TUNEL) staining. Scale bar = 25  $\mu$ m. **(G)** Quantitative analysis of cardiac fibrosis using Masson trichrome staining,  $n = 12$  fields per group. **(H)** Quantitative analysis of cross-sectional area of cardiomyocytes using WGA staining,  $n = 4$  mice per group. **(I)** Quantitative analysis of TUNEL-positive cells,  $n = 15$  to 20 fields per group. **(J, K)** Representative immunoblots and quantitative data of ANP, BNP,  $\beta$ -MHC, and GAPDH (loading control) in murine cardiac tissues,  $n = 6$  mice per group. Data are shown as mean  $\pm$  SEM. Multiple groups were compared with 1-way analysis of variance followed by Tukey's post hoc test. \* $P < 0.05$ , \*\* $P < 0.01$ , and \*\*\* $P < 0.001$  vs the Sham-NC or TAC-NC group. Abbreviations as in **Figures 1 and 2**.

**FIGURE 5** Cardiac STX17 Overexpression Alleviated TAC-Induced Mitochondrial Damage in Cardiomyocytes



**(A)** Representative and quantitative analysis of adult mouse cardiomyocyte loaded with TMRM to detect mitochondrial membrane potential in AAV-NC and AAV-STX17 mice with or without TAC surgery. Scale bar = 25 μm, n = 16 fields per group. **(B)** Representative and quantitative analysis of adult mouse cardiomyocytes loaded with MitoSOX. Scale bar = 25 μm, n = 16 fields per group. **(C)** Representative immunoblots and quantitated data of OXPHOS in murine cardiac tissues, n = 5 mice per group. **(D, E)** Representative transmission electron microscopy images and quantitative analysis of mitochondrial morphology. Scale bars = 2 μm or 500 nm, n = 4 to 6 mice per group. **(F-H)** Quantitated data of oxygen consumption rate in adult mouse cardiomyocytes isolated from AAV-NC and AAV-STX17 mice with or without TAC surgery. Data are shown as mean ± SEM. Multiple groups were compared with 1-way analysis of variance followed by Tukey's post hoc test. \**P* < 0.05, \*\**P* < 0.01, and \*\*\**P* < 0.001 vs the Sham-NC or TAC-NC group. ATP = adenosine triphosphate; OCR = oxygen consumption rate; other abbreviations as in **Figures 1, 2, and 4**.

**FIGURE 6 STX17 Overexpression Improved Mitochondrial Function via DRP1-Dependent Mitophagy**



noted in mice following TAC surgery, the effect of which was alleviated by STX17 overexpression (Figures 6A and 6B). Moreover, evaluation of PARKIN levels in mitochondrial fractions revealed down-regulated mitophagy marker in TAC-induced HF, the effect of which was ameliorated by STX17 overexpression (Supplemental Figure 8A). Similarly, relative mitochondrial DNA content was overtly increased in hearts with TAC surgery, the effect of which was reversed by STX17 overexpression (Supplemental Figure 4K).

To verify whether STX17 promotes mitophagy in TAC-induced HF, 3-MA was administered to inhibit autophagosome formation in mice upon TAC surgery with or without STX17 overexpression.<sup>30</sup> Our data showed that 3-MA administration cancelled off the STX17-offered protective role on cardiac function as manifested by ejection fraction, fractional shortening, left ventricular end-diastolic volume, left ventricular end-systolic volume, and interstitial fibrosis in mice with TAC-induced HF (Figures 6C to 6F). Furthermore, our results also revealed a downregulated mt-keima ratio, LC3II levels in mitochondrial fractions, levels of autophagosomes and autolysosomes, and mitochondrial membrane potential in adult mouse cardiomyocytes from mice with TAC-induced HF, the effects of which were alleviated in response to STX17 overexpression. However, 3-MA treatment cancelled off the protective role of STX17 on mitophagy and mitochondrial function in TAC-induced HF (Figures 6G and 6J, Supplemental Figures 8B to 8D).

Moreover, Baf A1, a lysosomal V-ATPase inhibitor interrupting autophagy flux, was used to discern the effect of STX17 on promoting mitophagy in cardiomyocytes upon PE challenge.<sup>30</sup> Western blot analysis indicated that total mitochondrial LC3II levels were dramatically increased in response to Baf A1 under normal environment. Upon PE challenge,

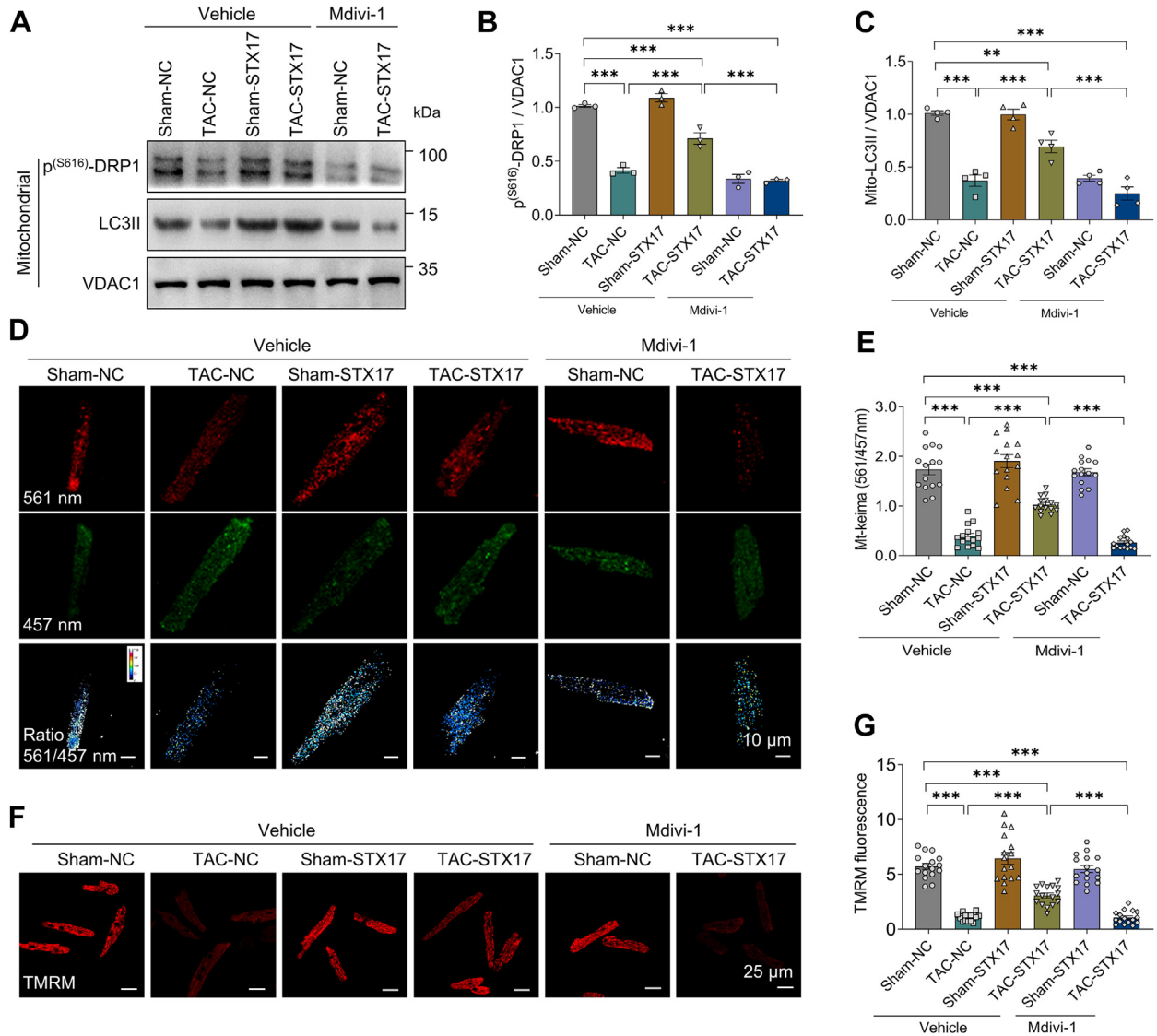
Baf A1 failed to induce total and mitochondrial LC3II rises in neonatal mouse cardiomyocytes, although such an effect was recovered by STX17 overexpression (Supplemental Figures 9A to 9C). Then, neonatal mouse cardiomyocytes transfected with mRFP-GFP-LC3 adenovirus were subjected to PE challenge with or without Baf A1 treatment. Our data revealed that both autophagosomes (mRFP-GFP-LC3, yellow dots) and autolysosomes (mRFP-LC3, red dots) were significantly decreased following PE stress. STX17 overexpression significantly increased autophagosomes accompanied by an increase in autolysosomes. Baf A1 increased autophagosomes (but not autolysosomes) in neonatal mouse cardiomyocytes under control condition. However, it failed to induce rises in autophagosomes under PE stress, the effects of which were drastically alleviated by STX17 overexpression under PE condition (Supplemental Figures 9D and 9E). These results suggested that STX17 overexpression countered PE-evoked suppression of autophagy and mitophagy flux.

Moreover, mdivi-1, a DRP1 GTPase inhibitor, was employed to evaluate potential involvement of DRP1 in STX17-induced mitophagy response in HF. Our results showed that mitochondrial LC3II and p(S616)-DRP1 levels were suppressed in adult mouse cardiomyocytes upon TAC challenge, the effect of which were attenuated by STX17 overexpression (Figures 7A to 7C). Interestingly, mdivi-1 overtly inhibited the effect of STX17 on promoting mitophagy. Consistently, mdivi-1 administration also cancelled off the improvement of STX17 on LC3II levels in the mitochondrial fractions, mito-Keima ratio, and collapsed mitochondrial membrane potential in TAC-induced mitochondrial dysfunction (Figures 7D to 7G). These findings indicated that protection of STX17 overexpression on mitochondrial function was mediated by DRP1-dependent mitophagy.

**FIGURE 6 Continued**

(A, B) Representative immunoblots and quantitative data of DRP1, p(S616)-DRP1, p(S637)-DRP1, GAPDH (loading control), LC3, P62, and VINCULIN (loading control) in the whole-cell lysates; p(S616)-DRP1, p(S637)-DRP1, VDAC1 (loading control), LC3II, and VDAC1 (loading control) in the mitochondrial fractions; and p(S616)-DRP1 and CNX (loading control) in the MAM fractions in the heart tissues, n = 6 mice per group. Male C57BL/6J mice were intravenously injected with AAV-STX17 with cardiac troponin T promoter at the dose of  $5 \times 10^{11}$  plaque-forming units and were randomly assigned to the sham group or TAC group for 4 weeks. Mice were intraperitoneally injected with 3-methyladenine (3-MA) (15 mg/kg) every 3 days after TAC surgery. (C, D) Representative echocardiographic images and quantitative data including EF, FS, LVEDV, and LVESV, n = 4 to 6 mice per group. (E, F) Representative images and quantitative analysis of cardiac fibrosis using Masson trichrome staining (scale bar = 50  $\mu$ m), n = 15 fields per group. Adult mouse cardiomyocytes were isolated from AAV-NC and STX17 overexpression mice with or without TAC surgery and 3-MA treatment. (G, H) Representative confocal microscopic images and quantitative data of mt-keima; AMCMs were transduced with mt-keima adenovirus (multiplicity of infection = 20) for 48 hours, n = 20 fields per group. (I, J) Representative confocal microscopic images and quantitative data of TMRM staining, n = 12 fields per group. Data are shown as mean  $\pm$  SEM. Multiple groups were compared with 1-way analysis of variance followed by Tukey's post hoc test. \*P < 0.05, \*\*P < 0.01, and \*\*\*P < 0.001 vs the Sham-NC, TAC-NC, or TAC-STX17 group. Abbreviations as in Figures 1, 2, 4, and 5.

**FIGURE 7** Midivi-1, a DRP1 GTPase Inhibitor, Cancelled off the Protective role of STX17 Overexpression on Mitophagy and Mitochondrial Function in TAC-Induced HF

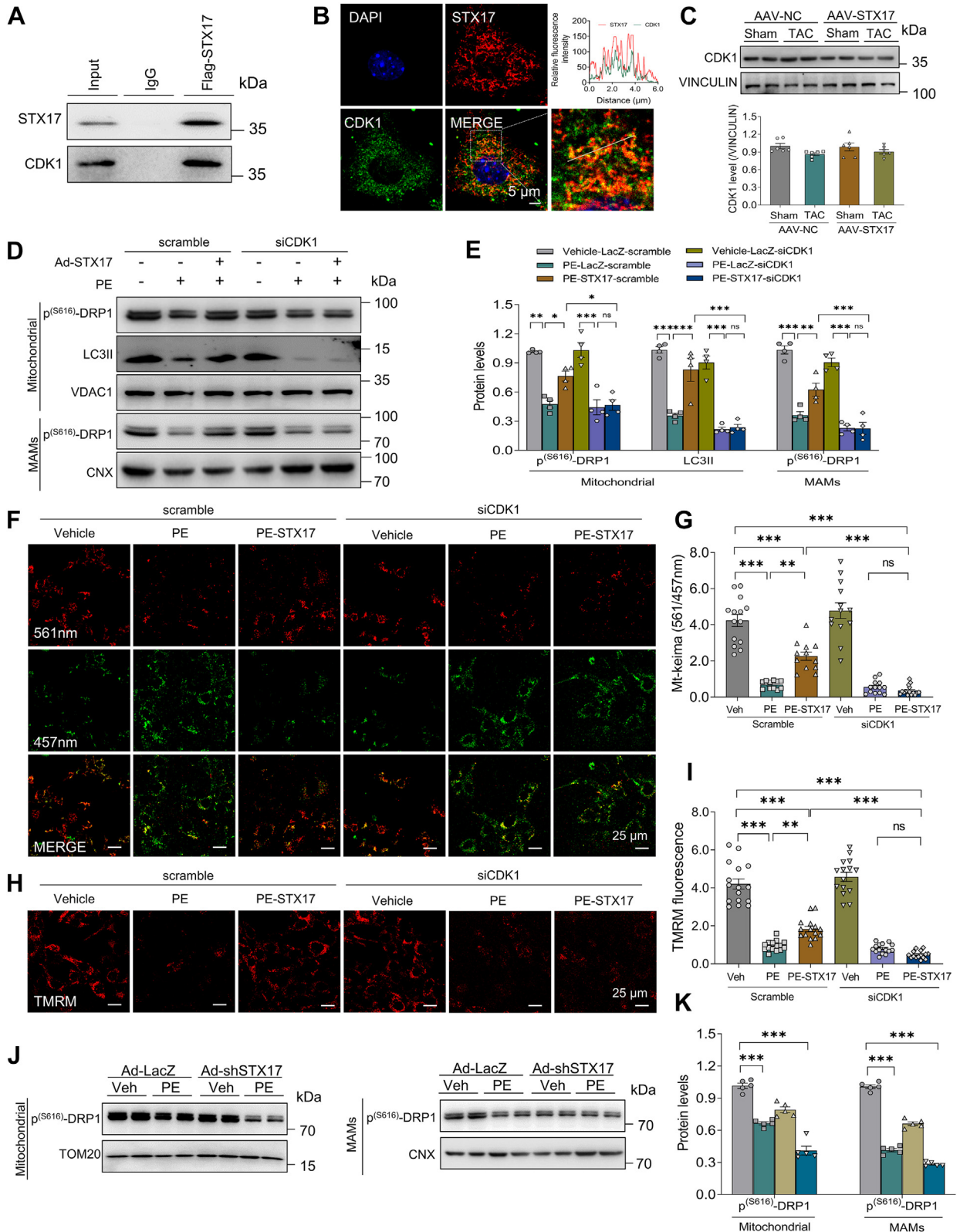


Adult mouse cardiomyocytes were isolated from AAV-NC and STX17 overexpression mice with or without TAC surgery. Mdivi-1 (10  $\mu$ M) was added for 24 hours to inhibit the phosphorylation of DRP1. **(A-C)** Representative immunoblots and quantitated data of p-(S616)-DRP1, LC3II, and VDAC1 (loading control) in the mitochondrial fractions of adult mouse cardiomyocytes, n = 3 to 4 per group. **(D, E)** Representative confocal microscopic images and quantitative data of mt-keima. Adult mouse cardiomyocytes were transduced with mt-keima adenovirus (multiplicity of infection = 20) for 24 hours, n = 20 fields per group. **(F, G)** Representative confocal microscopic images and quantitative data of TMRM, n = 16 fields per group. Data are shown as mean  $\pm$  SEM. Multiple groups were compared with 1-way analysis of variance followed by Tukey's post hoc test. **\*\*P** < 0.01 and **\*\*\*P** < 0.001 vs the Sham-NC, TAC-NC, or TAC-STX17 group. Abbreviations as in **Figures 1, 2, 4, and 5**.

**STX17 RECRUITED CDK1 TO PHOSPHORYLATE DRP1 AT SER616 AND TRANSLOCATE TO MAMs IN CARDIOMYOCYTES.** Multiple kinases including CDK1,<sup>33</sup> receptor-interacting serine/threonine protein kinase 1,<sup>34</sup> extracellular signal-regulated kinase,<sup>35</sup> and Ca<sup>2+</sup>/calmodulin-dependent kinase II<sup>36</sup> have been reported to phosphorylate DRP1 at Ser616. Given

that the protective role of STX17 on HF was related to the phosphorylation and mitochondrial translocation of DRP1, it is pertinent to identify candidate kinase recruited by STX17 in MAMs. Then, immunoprecipitation followed by a mass spectrometry experiment in the lysates of neonatal mouse cardiomyocytes transduced with Ad-Flag-STX17 was performed. Thus,

**FIGURE 8** STX17 Promoted the Phosphorylation of DRP1 at Ser616 and Translocation to MAMs Through Recruiting CDK1 in Cardiomyocytes



CDK1 was identified based on precipitated protein list (Supplemental Table 2). To confirm the interaction between STX17 and CDK1, coimmunoprecipitation using Ad-Flag-STX17 overexpression in neonatal mouse cardiomyocytes was examined. Our results indicated that STX17 could indeed interact with CDK1 (Figure 8A). In addition, the colocalization between STX17 and CDK1 in neonatal mouse cardiomyocytes also confirmed this interaction (Figure 8B). Furthermore, it was revealed that TAC surgery did not exert significant effect on the levels of CDK1 in the presence or absence of STX17 overexpression (Figure 8C).

To verify if CDK1 plays an obligatory role in STX17-induced redistribution of DRP1, localization of DRP1 and p(S616)-DRP1 was examined in AC16 cells with CDK1 knockdown in the presence or absence of PE challenge. Strikingly, CDK1 knockdown cancelled off STX17-elicited protective effect on MAM translocation and phosphorylation of p(S616)-DRP1, as well as changes in LC3II and p(S616)-DRP1 in mitochondrial fractions upon PE challenge (Figures 8D and 8E). Meanwhile, STX17 overexpression preserved mitophagy and mitochondrial membrane potential under PE stimulation, although these effects were absent in AC16 cells with CDK1 knockdown (Figures 8F to 8I, Supplemental Figure 6B). These results favor an obligatory role of CDK1 in STX17-mediated cardiac protection in the face of PE challenge.

Moreover, to understand if CDK1-mediated phosphorylation and redistribution of DRP1 at MAMs is dependent on STX17, protein levels of CDK1 were evaluated between *Stx17<sup>fl/fl</sup>* and *Stx17<sup>cko</sup>* mice. Our data showed that STX17 deletion did not affect the expression levels of CDK1 in heart tissues. Then, due to extremely higher mortality of *Stx17<sup>cko</sup>* mice during the perioperative period of TAC surgery, Ad-shSTX17 was constructed to knockdown STX17 in adult mouse cardiomyocytes with or without PE treatment (Supplemental Figures 6C and 6D). Our data revealed that PE challenge reduced levels of p(S616)-DRP1 in

mitochondrial and MAM fractions, with a pronounced decrease in Ad-shSTX17 transduced cells with PE stress. STX17 knockdown alone also inhibited levels of p(S616)-DRP1 in mitochondrial and MAM fractions, particularly in MAM fractions (Figures 8J and 8K). These results indicated that endogenous STX17 played a crucial role to promote CDK1-mediated redistribution of DRP1 on MAMs followed by S616 phosphorylation of DRP1.

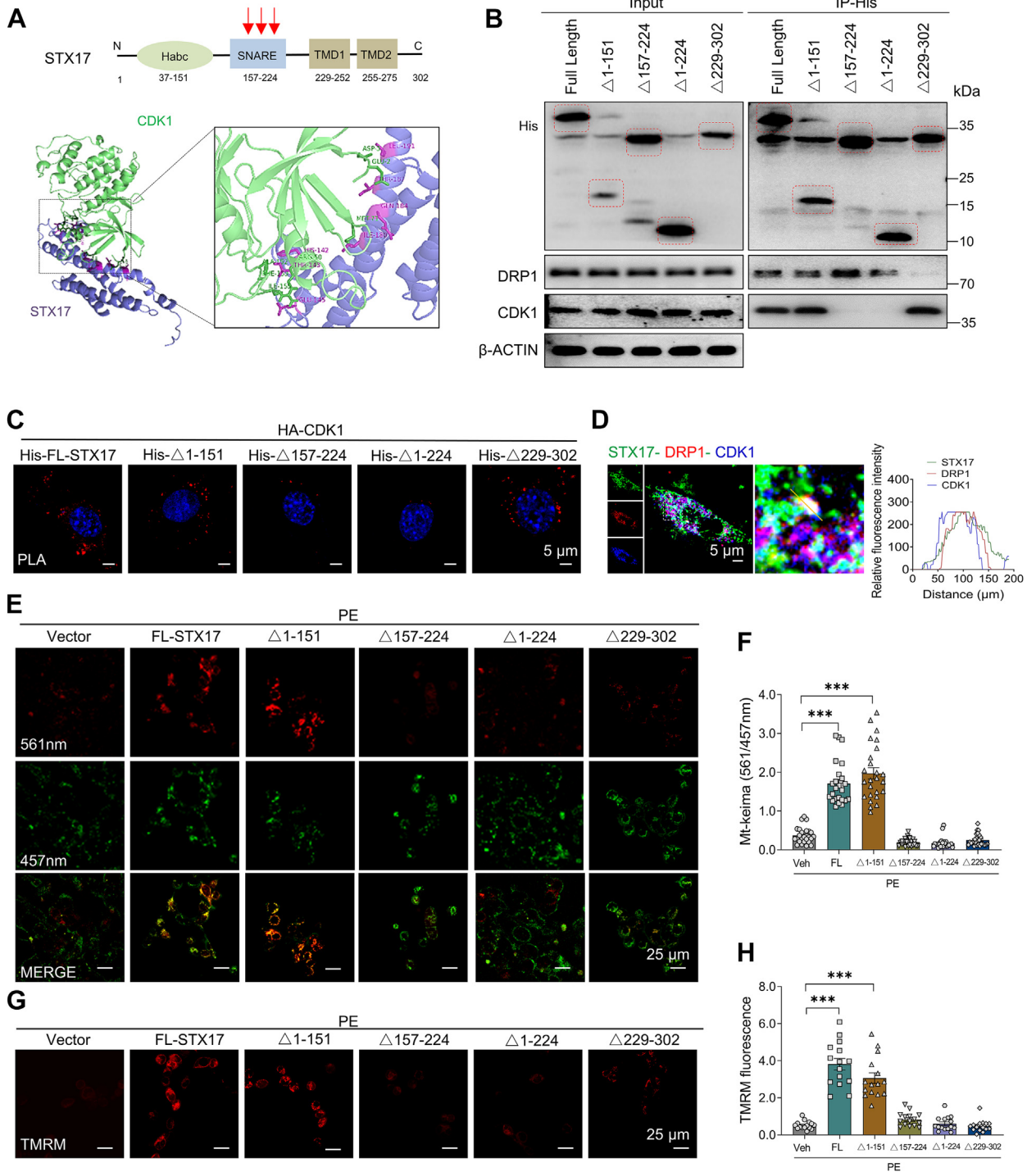
**STX17 INTERACTED WITH CDK1 THROUGH ITS SNARE DOMAIN, WHICH IS DIFFERENT FROM ITS BINDING SITES WITH DRP1.** Given that STX17 interacted with both CDK1 and DRP1, its binding domains for CDK1 or DRP1 warrant to be elaborated. STX17 contains distinct domains including Habc binding (aa 1-151), SNARE binding (aa 157-224), and TEM-CHD domains (aa 229-302) (Figure 9A).<sup>37</sup> Thus, His-tagged STX17 mutants targeting these domains including  $\Delta$ 1-151,  $\Delta$ 157-224,  $\Delta$ 1-224, and  $\Delta$ 229-302 were constructed for coimmunoprecipitation assays. It was demonstrated that STX17 interacted with DRP1 via its C-terminal cytoplasmic tail.<sup>21</sup> Our data confirmed DRP1 interacted with His-tagged STX17 full length,  $\Delta$ 1-151,  $\Delta$ 157-224, and  $\Delta$ 1-224 in AC16 cells, indicating that DRP1 would interact with the TEM-CHD domain of STX17 (Figure 9B).

Then, our prediction of STX17 interacting sites on CDK1 suggested localization of binding segments within Habc or SNARE domains, with the SNARE domain possessing a higher probability. AC16 cells were transfected with various truncated variants of His-STX17 plasmids and HA-tagged CDK1 plasmids. Coimmunoprecipitation and PLA analysis revealed that segment of STX17 (aa 157-224) was responsible for STX17-CDK1 interaction without any contribution from segments of STX17 (aa 1-157) and STX17 (aa 229-302) (Figures 9B and 9C). Moreover, formation of the complex of STX17, CDK1, and DRP1 was confirmed by colocalization of immunofluorescence analysis in AC16 cells (Figure 9D).

#### FIGURE 8 Continued

(A) Representative immunoprecipitation blots with an anti-Flag or an anti-cyclin-dependent kinase-1 (anti-CDK1) antibody in neonatal mouse cardiomyocytes transfected with Ad-Flag-STX17 for 48 hours. (B) Representative immunofluorescence images and plot profile analysis of STX17 and CDK1. Scale bar = 5  $\mu$ m. Neonatal mouse cardiomyocytes were transduced with Ad-Flag-STX17 adenovirus at the multiplicity of infection of 20 for 24 hours. (C) Representative immunoblots and quantitative data of CDK1 and GAPDH (loading control) in murine cardiac tissues, n = 6. (D, E) Representative immunoblots and quantitative data of DRP1, p(S616)-DRP1, LC3II, and TOM20 (loading control) in the mitochondrial fractions and p(S616)-DRP1 and CNX (loading control) in the MAM fractions of AC16 cells. AC16 cells were transfected with scramble and small interfering CDK1 for 48 hours, in prior to Ad-STX17 transduction for 24 hours with or without PE treatment (48 hours), n = 4. (F, G) Representative images and quantitative data of mt-keima. Scale bar = 25  $\mu$ m, n = 15 fields from 3 independent experiments. (H, I) Representative images and quantitative data of TMRM. Scale bar = 25  $\mu$ m, n = 15 fields from 3 independent experiments. (J, K) Representative immunoblots and quantitative data of p(S616)-DRP1 and TOM20 (loading control) in the mitochondrial fractions and p(S616)-DRP1 and CNX (loading control) in the MAM fractions of AC16 cells. AC16 cells were transduced with Ad-LacZ and Ad-shSTX17 for 24 hours with or without PE treatment (48 hours), n = 4. Data are shown as mean  $\pm$  SEM. Multiple groups were compared with 1-way analysis of variance followed by Tukey's post hoc test, \*P < 0.05, \*\*P < 0.01 and \*\*\*P < 0.001. Abbreviations as in Figures 1 to 5.

**FIGURE 9** STX17 Interacted With CDK1 and DRP1 Through Different Domains



Continued on the next page

Next, mt-keima and TMRM were determined in PE-challenged AC16 cells in the presence of truncated plasmids. Data in **Figures 9E and 9F** showed that STX17 full length overexpression significantly increased mt-keima activity compared with that subjected to PE stimulation, with a similar response in  $\Delta 1$ -151 overexpression. Deletion of STX17 ( $\Delta 157$ -224,  $\Delta 1$ -224, and  $\Delta 229$ -302) failed to duplicate STX17 full length) evoked responses. Furthermore, TMRM analysis showed that STX17 full length and  $\Delta 1$ -151 overtly preserved mitochondrial membrane potential decline upon PE treatment, with a pronounced decline in STX17 ( $\Delta 157$ -224,  $\Delta 1$ -224 and  $\Delta 229$ -302) group, indicating the STX17 mutant ( $\Delta 157$ -224 and  $\Delta 229$ -302) failed to alleviate collapsed mitochondrial membrane potential in AC16 cells upon PE stress (**Figures 9G and 9H**). Taken together, STX17 interacted with CDK1 through its SNARE domain but with DRP1 through its C-terminal tails, both of which play critical roles in mediating DRP1-dependent mitophagy.

**CDK1 INHIBITOR COUNTERACTED CARDIAC PROTECTION OF STX17 IN TAC-INDUCED HF.** Given that CDK1 was a prerequisite for STX17-mediated cardioprotection in TAC-induced HF, a CDK1 inhibitor was used to further elucidate the mechanism of STX17 in vivo. C57BL/6J mice (6 weeks) were injected with AAV9-cTNT-STX17 via tail vein prior to TAC surgery. AZD5438, a CDK1 inhibitor, was oral administered at the dosage of 50 mg/kg twice daily for 3 days following TAC surgery (**Figure 10A**). Four weeks after TAC, echocardiographic analysis revealed that AZD5438 nullified the protective effect of STX17 overexpression on ejection fraction, fractional shortening, left ventricular end-diastolic diameter, and left ventricular end-systolic diameter in mice with TAC-induced HF (**Figures 10B and 10C**). Furthermore, TAC-induced morphological enlargement in the heart was alleviated by STX17 overexpression, albeit it was aggravated by AZD5438. A similar effect was observed in cardiac fibrosis with Masson trichrome staining and cross-sectional area of cardiomyocytes using wheat germ agglutinin staining (**Figures 10D to 10F**). Our results also revealed that AZD5438 administration nullified the beneficial effect

of STX17 overexpression on mitophagy and mitochondrial membrane potential levels with mt-keima detection and TMRM staining (**Figures 10G to 10J**). Moreover, AZD5438 cancelled off the STX17-offered benefit against TAC-induced HF, including elevation of LC3II and LC3I levels in whole-cell lysates, LC3II and p(S616)-DRP1 levels in mitochondrial fractions, and p(S616)-DRP1 levels in MAMs. These results indicated that AZD5438 cancelled off the beneficial effect of STX17 overexpression against TAC-induced HF through inhibiting CDK1/DRP1-mediated mitophagy (**Supplemental Figures 10A to 10C**).

In addition, we also scrutinized levels of autophagy markers, p(S616)-DRP1, and CDK1 in the whole-cell lysates and mitochondrial fractions of heart tissues from patients with HF. In line with the aforementioned results, our data revealed that LC3II protein levels were reduced while P62 levels were increased in hearts of patients with HF compared with nonfailing myocardium. DRP1, p(S616)-DRP1, p(S637)-DRP1, and CDK1 levels seemed to be comparable in whole-cell lysates of hearts with or without HF. However, LC3II, PARKIN, and p(S616)-DRP1 were significantly downregulated in mitochondrial fractions of failing hearts (**Supplemental Figures 11A to 11C**). These data also support involvement of DRP1-mediated mitophagy in the progression of HF.

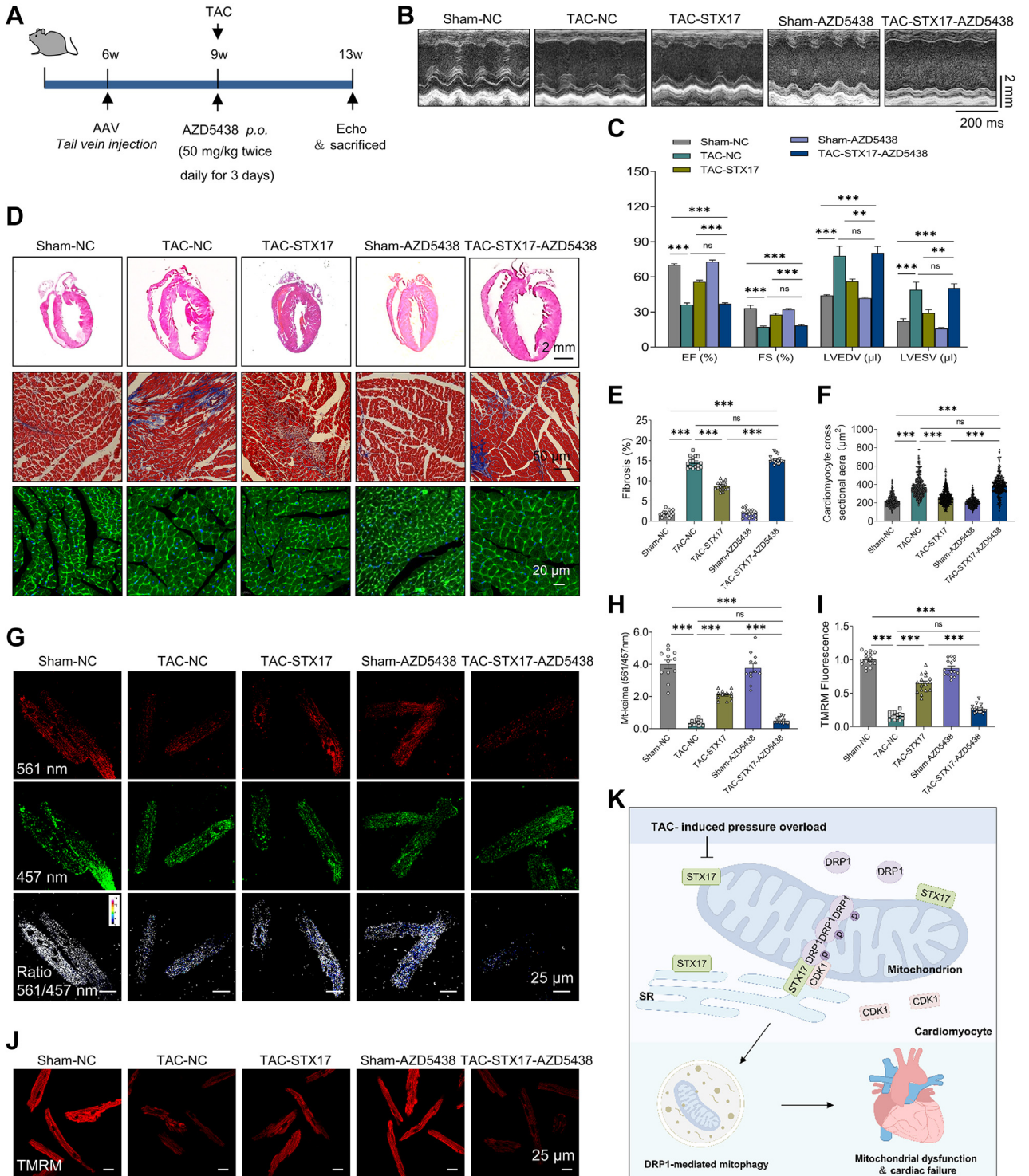
## DISCUSSION

Salient findings from our study noted a cardioprotective role for STX17 against TAC-induced HF. Our data revealed downregulated STX17 in human myocardium with HF and in murine hearts following TAC. Cardiac-specific STX17 knockout resulted in mitochondrial dysfunction in murine hearts by inhibiting phosphorylation and MAM translocation of DRP1, ultimately repressing DRP1-dependent mitophagy. Our results revealed that STX17 effectively rescued phosphorylation and redistribution of DRP1 in MAMs to attenuate TAC-induced HF by improving cardiac mitophagy and mitochondrial dysfunction. Mechanistically, STX17 recruited the kinase CDK1 through its SNARE domain to

### FIGURE 9 Continued

**(A)** Schematic description of STX17 domain mutants. Cartoon represents the predicted STX17-CDK1 complex structure. **(B)** Representative immunoprecipitation blots with an anti-His antibody, anti-DRP1 or anti-HA antibody in AC16 cells transfected with pcDNA3.1(+)-HA-CDK1, as well as His-STX17 full length, His-STX17 ( $\Delta 1$ -151), His-STX17 ( $\Delta 157$ -224), His-STX17 ( $\Delta 1$ -224), or His-STX17 ( $\Delta 229$ -302) for 48 hours. **(C)** Representative images of PLA analysis for His and HA antibodies. **(D)** Representative immunofluorescence images and plot profile analysis of colocalization of STX17, CDK1, and DRP1. AC16 cells were transfected with pcDNA3.1(+)-HA-CDK1 and his-STX17 for 48 hours. **(E, F)** Representative images and quantitated data of mt-keima. AC16 cells transfected with pcDNA3.1(+)-His-STX17 full length, His-STX17( $\Delta 1$ -151), His-STX17( $\Delta 157$ -224), His-STX17( $\Delta 1$ -224), or His-STX17( $\Delta 229$ -302) for 48 hours following with PE treatment. Scale bar = 25  $\mu$ m, n = 20 to 30 fields per group from 3 independent experiments. **(G, H)** Representative images and quantitated data of TMRM staining. Scale bar = 25  $\mu$ m, n = 20 to 30 fields per group from 3 independent experiments. Data are shown as mean  $\pm$  SEM. Multiple groups were compared with 1-way analysis of variance followed by Tukey's post hoc test. \*\*\**P* < 0.001. Abbreviations as in **Figures 1 to 5** and **8**.

**FIGURE 10** CDK1 Inhibitor Counteracted Cardiac Protection of STX17 in TAC-Induced HF



phosphorylate DRP1 at Ser616 in MAMs, which subsequently promoting mitophagy in cardiomyocytes. Herein, these findings favored a new therapeutic option of STX17 in the progression of HF by reversing DRP1-dependent mitophagy (Figure 10K).

Cumulative evidence has suggested that STX17 orchestrated the development of autophagy by different combinative partners.<sup>38,39</sup> STX17 also exerts pleiotropic roles in mitochondrial quality control, including mitochondrial dynamics,<sup>22</sup> mitochondrial Ca<sup>2+</sup> homeostasis,<sup>22,39</sup> mitophagic activity,<sup>18,21</sup> and even lipid metabolism.<sup>40</sup> Findings from the present study revealed that cardiac STX17 deletion alone resulted in cardiac ventricular dysfunction and remodeling, which might be on account of mitochondrial damage, evidenced by the increased MitoSOX intensity, reduced mitochondrial membrane potential, and impairment of mitophagy, consistent with previous findings.<sup>41</sup> In contrast, targeting STX17 may provide protective response on mitophagy in retarding the HF progress. This notion received support from our data in that cardiomyocyte-specific overexpression of STX17 using AAV9-mediated delivery significantly improved cardiac dysfunction and mitochondrial function without exhibiting notable adverse effects. AAV-mediated STX17 delivery may help to provide a promising target therapy for cardiac dysfunction.

Mitophagy, the most important machinery for elimination of dysfunctional mitochondria, is essential to ensuring cardiomyocyte function and survival.<sup>10,42</sup> Our work demonstrated that endogenous STX17 deletion in cardiomyocytes resulted in mitophagic decline and subsequently mitochondrial damage, while STX17 overexpression promoted mitophagy and improved mitochondrial integrity in TAC-induced HF. In addition, it was reported that mitophagy was transiently activated prior to a gradual decline in response to pressure overload-induced HF.<sup>14</sup> Likewise, phosphorylation at Ser616 and mitochondrial translocation of DRP1 were found

to be upregulated 3 to 5 days following TAC surgery and were suppressed thereafter, suggesting a temporal association of mitophagic activity in myocardium following TAC stress.<sup>11</sup> Our study also revealed that STX17 protein levels were transiently elevated before a gradual decline in hearts following TAC surgery, with a similar tendency of DRP1-dependent mitophagy. These findings suggested a compensatory cardioprotective role for STX17, likely involving DRP1-dependent mitophagy.

Recently, the role of DRP1 in the regulation of cardiac homeostasis has been intensively examined.<sup>43,44</sup> Cardiac homozygous deletion of DRP1 resulted in lethal cardiomyopathy in mice.<sup>16</sup> Cardiac DRP1 haploinsufficiency revealed dilated cardiomyopathy with accumulation of damaged mitochondria,<sup>16</sup> suggesting a pivotal role for endogenous DRP1 in maintaining mitophagy and mitochondrial homeostasis in the heart. Mitochondrial dysfunction and ventricular failure were also observed in tamoxifen-inducible cardiac-specific DRP1 knockout mice.<sup>11</sup> In agreement with these findings, our data also supported an essential role for DRP1-dependent mitophagy and mitochondrial quality control in the development of TAC-induced HF. Previous work revealed the complexity of DRP1 in mitochondrial quality control based on its translocation to mitochondria. DRP1 binds to different proteins on the outer mitochondrial membrane to facilitate its translocation from cytoplasm to mitochondria, to participate in the regulation of mitochondrial homeostasis.<sup>45</sup> For example, DRP1 mediates frequent mitochondrial fission, allowing mitophagic degradation of damaged (depolarized) mitochondria in neurons and fibroblasts.<sup>46</sup> Nonetheless, given that mitochondria are relatively static and fragmented in adult cardiomyocytes with an extremely low frequency of mitochondrial division under baseline conditions, a noncanonical role of DRP1 on fission-independent functions has drawn some recent attentions.<sup>43,47</sup> Several evidence have indicated that DRP1 coordinates with various mitophagic

#### FIGURE 10 Continued

Male C57BL/6J mice were intravenously injected with AAV-STX17 at the dose of  $5 \times 10^{11}$  plaque-forming units and were randomly assigned to the sham or TAC group with or without AZD5438 administration (50 mg/kg twice daily for 3 days). (A) Schematic description of treated protocol in mice. (B, C) Representative echocardiographic images and quantitative data including EF, FS, LVEDV, and LVESV,  $n = 5$  mice per group. (D) Representative heart slices using H&E (scale bar = 2 mm), Masson trichrome (scale bar = 50  $\mu$ m), and WGA (scale bar = 20  $\mu$ m) staining. (E) Quantitative analysis of cardiac fibrosis using Masson trichrome staining,  $n = 15$  to 20 fields per group. (F) Quantitative analysis of cross-sectional area of cardiomyocytes using WGA staining,  $n = 4$  to 6 mice per group. (G, H) Representative confocal microscopic images and quantitative data of mt-keima. Adult mouse cardiomyocytes were transduced with mt-keima adenovirus (multiplicity of infection = 20) for 48 hours,  $n = 12$  fields per group. (I, J) Representative confocal microscopic images and quantitative data of TMRM staining,  $n = 15$  fields per group. Data are shown as mean  $\pm$  SEM. Multiple groups were compared with 1-way analysis of variance followed by Tukey's post hoc test. **\*\*** $P < 0.01$  and **\*\*\*** $P < 0.001$  vs the Sham-NC, TAC-NC, or TAC-STX17 group. (K) Schematic diagram depicting the role of STX17 in the progression of heart failure. TAC-induced pressure overload resulted in STX17 compensated insufficiency in myocardium, resulting in the reduction of CDK1 recruited to MAMs by STX17, which subsequently repressed the phosphorylation and MAM translocation of DRP1, ultimately suppressing DRP1-dependent mitophagy and inducing cardiac dysfunction. SR = sarcoplasmic reticulum; other abbreviations as in Figures 1 to 5 and 8.

molecules including PARKIN, BNIP3, and FUNDC1 to drive biogenesis and autophagy of mitochondria to sustain mitochondrial homeostasis.<sup>46,48,49</sup> It was recently reported that DRP1 could also bind with mitochondrial Zn transporter (Zip1) and collapse mitochondrial membrane potential, thus facilitating defective mitochondria for selective elimination.<sup>50</sup> Given the complicate and multifaceted role of DRP1, our data exhibited that the DRP1 recruited to the MAM region by STX17 was involved in the protective mechanism of mitophagy in TAC-induced HF. Further investigation is warranted to confirm the effect of DRP1 on mitophagy in the heart, as well as the precise molecular mechanism involved.

In addition, although several studies have depicted that increased mitochondrial fission in hearts subjected to acute ischemic stresses, while Drp1 inhibitors including mdivi-1 and P110 (which inhibits interaction of Fis1 and DRP1) alleviated mitochondrial fission and cardiac dysfunction and proved to be protective for short-term treatment in myocardial ischemic injury.<sup>16,51,52</sup> More caution is needed for the application of DRP1 inhibitors for prolonged periods of therapy against chronic progress of HF, owing to its primary effect on mitophagy and an essential role for normal cardiac function.

STX17 was involved in the regulating the phosphorylation and localization of DRP1 through various kinases. STX17 was reported to facilitate dephosphorylation of DRP1 by regulating phosphatase phosphoglycerate mutase family member 5.<sup>21</sup> Additionally, STX17 was found to govern the DRP1 activity by competing with Rab32, the protein kinase A anchoring protein, to prevent protein kinase A-mediated phosphorylation of DRP1 at Ser637.<sup>22</sup> However, both previous reports and our data showed no apparent change in the levels of total DRP1 and p(S637)-DRP1 in TAC-induced HF with or without STX17 overexpression. These results indicated that the mechanism of STX17 involving in the phosphorylation of DRP1 might be associated with other kinases in the progression of HF. Then, CDK1 was identified as a possible kinase recruited to MAMs by STX17 because it is the top kinase on the list of immunoprecipitation followed by liquid chromatography mass spectrometry analysis in Ad-STX17 cell lysates. Thus, the interaction between STX17 and CDK1 was further validated using co-immunoprecipitation, immunofluorescence, and the domain mutant mapping techniques. Our in vitro study also demonstrated that STX17 (full length) transfection mediated pronounced improvement of mitophagic flux and mitochondrial function in cardiomyocytes under PE stress, the effect of which was

abrogated in STX17 mutants ( $\Delta$ 157-224,  $\Delta$ 1-224, and  $\Delta$ 229-302). Furthermore, CDK1 knockdown or inhibition offset the protective effect of STX17 on promoting DRP1-dependent mitophagy and preserve mitochondrial function in cardiomyocytes under PE stimulation or TAC stress both in vitro and in vivo. Moreover, we also demonstrated that STX17 is a prerequisite for the effect of CDK1 on phosphorylation and translocation onto MAMs of DRP1. The evidence was that loss of STX17 abrogated the effect of CDK1 on the phosphorylation of DRP1 at Ser616 in MAMs and mitochondrial fractions. It was concluded that phosphorylation at Ser616 of DRP1 through STX17-CDK1 complex in MAMs is crucial for the mitophagic activity to prevent the pathophysiological process of HF. Furthermore, we also investigated the levels of CDK1 and DRP1-mediated mitophagy in the hearts of HF patients. Our data revealed the suppression of STX17 levels and DRP1-mediated mitophagic activity, which supported the involvement of STX17-CDK1-DRP1-mediated mitophagy in the progression of HF. These findings provide a novel therapeutic target by upregulating STX17 in the development of HF.

**STUDY LIMITATIONS.** First, cardiomyocyte *Stx17<sup>cko</sup>* mice generated using *Stx17<sup>fl/fl</sup>* bred with *Myh6-cre/ERT2* transgenic mice would be needed to further discern the role of STX17 in cardiac and mitochondrial function. Next, STX17 was shown to bind with CDK1 through its SNARE domain. Whether STX17 was phosphorylated by CDK1 and got involved in DRP1-mediated mitophagy remains unclear. More concrete structural details would be needed with more site-specific mutation studies. Finally, specific mitophagy agonists are required to discern whether mitophagy activation can rescue cardiac dysfunction in *Stx17<sup>cko</sup>* mice.

## CONCLUSIONS

The current study elucidated that STX17 recruited the kinase CDK1, which offered a prerequisite for phosphorylation and redistribution in MAMs of DRP1, resulting in alleviating mitochondrial damage through facilitating mitophagy. These findings have suggested the therapeutic promises of targeting STX17 in the mitigation of TAC-induced HF. Future study is warranted to develop specific drugs modulating STX17 expression or function in the progression of HF.

**ACKNOWLEDGMENTS** Drs Haixia Xu, Xiang Wang and Wenjun Yu contributed equally to this work and were involved in study design, data collection, data analysis and editing the manuscript. Drs Shiqun Sun and Ne N. Wu provided technical assistance. Dr Junbo

Ge offered helpful discussion. Drs Jun Ren and Yingmei Zhang conceived the study and approved the manuscript.

Zhongshan Hospital, Fudan University, Shanghai 200032, China. E-mail: [ge.junbo@zs-hospital.sh.cn](mailto:ge.junbo@zs-hospital.sh.cn).

## FUNDING SUPPORT AND AUTHOR DISCLOSURES

This work was supported in part by the National Natural Science Foundation of China (82100277, 82130011, 92249301, 81900233, and 81770261), the Fundamental Research Funds for the Central Universities (2042022kf1125), and the Outstanding Young and Middle-aged Talents Training Program of Zhongnan Hospital of Wuhan University (Grant No. ZNYQ2022002). The authors have reported that they have no relationships relevant to the contents of this paper to disclose.

**ADDRESS FOR CORRESPONDENCE:** Dr Jun Ren, Shanghai Institute of Cardiovascular Diseases, Zhongshan Hospital, Fudan University, Shanghai 200032, China. E-mail: [jren\\_aldh2@outlook.com](mailto:jren_aldh2@outlook.com). OR Dr Yingmei Zhang, Shanghai Institute of Cardiovascular Diseases, Zhongshan Hospital, Fudan University, Shanghai 200032, China. E-mail: [zhangym197951@126.com](mailto:zhangym197951@126.com). OR Dr Junbo Ge, Shanghai Institute of Cardiovascular Diseases,

## PERSPECTIVES

**COMPETENCY IN MEDICAL KNOWLEDGE:** This study highlights that DRP1-mediated mitophagy is one of the major mechanisms for maintaining mitochondrial function in TAC-induced HF. STX17 recruits CDK1 onto MAMs and phosphorylates DRP1 at Ser616 to promote mitophagy, resulting in the preservation of contractile function in cardiomyocytes.

**TRANSLATIONAL OUTLOOK:** Future studies are warranted to determine the potential therapeutic benefit of STX17 and promotion of CDK1/DRP1-mediated mitophagy in cardiomyocytes for the prevention of cardiac remodeling and HF.

## REFERENCES

- McDonagh TA, Metra M, Adamo M, et al. 2021 ESC Guidelines for the diagnosis and treatment of acute and chronic heart failure. *Eur Heart J*. 2021;42:3599-3726.
- Zhou B, Tian R. Mitochondrial dysfunction in pathophysiology of heart failure. *J Clin Invest*. 2018;128:3716-3726.
- Bonora M, Wieckowski MR, Sinclair DA, Kroemer G, Pinton P, Galluzzi L. Targeting mitochondria for cardiovascular disorders: therapeutic potential and obstacles. *Nat Rev Cardiol*. 2019;16:33-55.
- Pickles S, Vigie P, Youle RJ. Mitophagy and quality control mechanisms in mitochondrial maintenance. *Curr Biol*. 2018;28:R170-R185.
- Rowland AA, Voeltz GK. Endoplasmic reticulum-mitochondria contacts: function of the junction. *Nat Rev Mol Cell Biol*. 2012;13:607-625.
- Zhou H, Wang S, Hu S, Chen Y, Ren J. ER-mitochondria microdomains in cardiac ischemia-reperfusion injury: a fresh perspective. *Front Physiol*. 2018;9:755.
- Li YE, Sowers JR, Hetz C, Ren J. Cell death regulation by MAMs: from molecular mechanisms to therapeutic implications in cardiovascular diseases. *Cell Death Dis*. 2022;13:504.
- Silva-Palacios A, Zazueta C, Pedraza-Chaverri J. ER membranes associated with mitochondria: possible therapeutic targets in heart-associated diseases. *Pharmacol Res*. 2020;156:104758.
- Shires SE, Gustafsson AB. Regulating renewable energy: connecting AMPKalpha2 to PINK1/Parkin-mediated mitophagy in the heart. *Circ Res*. 2018;122:649-651.
- Saito T, Hamano K, Sadoshima J. Molecular mechanisms and clinical implications of multiple forms of mitophagy in the heart. *Cardiovasc Res*. 2021;117:2730-2741.
- Shirakabe A, Zhai P, Ikeda Y, et al. Drp1-dependent mitochondrial autophagy plays a protective role against pressure overload-induced mitochondrial dysfunction and heart failure. *Circulation*. 2016;133:1249-1263.
- Wang B, Nie J, Wu L, et al. AMPKalpha2 protects against the development of heart failure by enhancing mitophagy via PINK1 phosphorylation. *Circ Res*. 2018;122:712-729.
- Cahill TJ, Leo V, Kelly M, et al. Resistance of dynamin-related protein 1 oligomers to disassembly impairs mitophagy, resulting in myocardial inflammation and heart failure. *J Biol Chem*. 2015;290:25907-25919.
- Miyamoto S, Brown JH. Drp1 and mitochondrial autophagy lend a helping hand in adaptation to pressure overload. *Circulation*. 2016;133:1225-1227.
- Song M, Franco A, Fleischer JA, Zhang L, Dorn GW 2nd. Abrogating mitochondrial dynamics in mouse hearts accelerates mitochondrial senescence. *Cell Metab*. 2017;26:872-883.e5.
- Ikeda Y, Shirakabe A, Maejima Y, et al. Endogenous Drp1 mediates mitochondrial autophagy and protects the heart against energy stress. *Circ Res*. 2015;116:264-278.
- Itakura E, Kishi-Itakura C, Mizushima N. The hairpin-type tail-anchored SNARE syntaxin 17 targets to autophagosomes for fusion with endosomes/lysosomes. *Cell*. 2012;151:1256-1269.
- Xian H, Yang Q, Xiao L, Shen HM, Liou YC. STX17 dynamically regulated by Fis1 induces mitophagy via hierarchical macroautophagic mechanism. *Nat Commun*. 2019;10:2059.
- Tian X, Teng J, Chen J. New insights regarding SNARE proteins in autophagosome-lysosome fusion. *Autophagy*. 2021;17:2680-2688.
- Viret C, Faure M. Regulation of syntaxin 17 during autophagosome maturation. *Trends Cell Biol*. 2019;29:1-3.
- Sugo M, Kimura H, Arasaki K, et al. Syntaxin 17 regulates the localization and function of PGAM5 in mitochondrial division and mitophagy. *EMBO J*. 2018;37:e98899.
- Arasaki K, Shimizu H, Mogari H, et al. A role for the ancient SNARE syntaxin 17 in regulating mitochondrial division. *Dev Cell*. 2015;32:304-317.
- Love MI, Huber W, Anders S. Moderated estimation of fold change and dispersion for RNA-seq data with DESeq2. *Genome Biol*. 2014;15:550.
- Wu T, Hu E, Xu S, et al. clusterProfiler 4.0: a universal enrichment tool for interpreting omics data. *Innovation (Camb)*. 2021;2:100141.
- Yu W, Sun S, Xu H, Li C, Ren J, Zhang Y. TBC1D15/RAB7-regulated mitochondria-lysosome interaction confers cardioprotection against acute

- myocardial infarction-induced cardiac injury. *Theranostics*. 2020;10:11244-11263.
26. Xu H, Yu W, Sun S, Li C, Ren J, Zhang Y. TAX1BP1 protects against myocardial infarction-associated cardiac anomalies through inhibition of inflammasomes in a RNF34/MAVS/NLRP3-dependent manner. *Sci Bull (Beijing)*. 2021;66:1669-1683.
27. Xu H, Yu W, Sun S, Li C, Zhang Y, Ren J. Luteolin attenuates doxorubicin-induced cardiotoxicity through promoting mitochondrial autophagy. *Front Physiol*. 2020;11:113.
28. Wu NN, Bi Y, Ajoalabady A, et al. Parkin insufficiency accentuates high-fat diet-induced cardiac remodeling and contractile dysfunction through VDAC1-mediated mitochondrial Ca(2+) overload. *J Am Coll Cardiol Basic Trans Science*. 2022;7:779-796.
29. Sun S, Yu W, Xu H, et al. TBC1D15-Drp1 interaction-mediated mitochondrial homeostasis confers cardioprotection against myocardial ischemia/reperfusion injury. *Metabolism*. 2022;134:155239.
30. Klionsky DJ, Abdel-Aziz AK, Abdelfatah S, et al. Guidelines for the use and interpretation of assays for monitoring autophagy (4th edition). *Autophagy*. 2021;17:1-382.
31. Wieckowski MR, Giorgi C, Lebedzinska M, Duszynski J, Pinton P. Isolation of mitochondria-associated membranes and mitochondria from animal tissues and cells. *Nat Protoc*. 2009;4:1582-1590.
32. Ren J, Sun M, Zhou H, et al. FUNDC1 interacts with FBXL2 to govern mitochondrial integrity and cardiac function through an IP3R3-dependent manner in obesity. *Sci Adv*. 2020;6:eabc8561.
33. Giovarelli M, Zecchini S, Martini E, et al. Drp1 overexpression induces desmin disassembling and drives kinesin-1 activation promoting mitochondrial trafficking in skeletal muscle. *Cell Death Differ*. 2020;27:2383-2401.
34. Saito T, Nah J, Oka SI, et al. An alternative mitophagy pathway mediated by Rab9 protects the heart against ischemia. *J Clin Invest*. 2019;129:802-819.
35. Prieto J, Leon M, Ponsoda X, et al. Early ERK1/2 activation promotes DRP1-dependent mitochondrial fission necessary for cell reprogramming. *Nat Commun*. 2016;7:11124.
36. Hu J, Zhang Y, Jiang X, et al. ROS-mediated activation and mitochondrial translocation of CaMKII contributes to Drp1-dependent mitochondrial fission and apoptosis in triple-negative breast cancer cells by isorhamnetin and chloroquine. *J Exp Clin Cancer Res*. 2019;38:225.
37. Li Y, Cheng X, Li M, et al. Decoding 3 distinct states of the Syntaxin17 SNARE motif in mediating autophagosome-lysosome fusion. *Proc Natl Acad Sci U S A*. 2020;117:21391-21402.
38. Zhou C, Wu Z, Du W, et al. Recycling of autophagosomal components from autolysosomes by the recycler complex. *Nat Cell Biol*. 2022;24:497-512.
39. Kumar S, Javed R, Mudd M, et al. Mammalian hybrid pre-autophagosomal structure HyPAS generates autophagosomes. *Cell*. 2021;184:5950-5969.e22.
40. Kimura H, Arasaki K, Ohsaki Y, et al. Syntaxin 17 promotes lipid droplet formation by regulating the distribution of acyl-CoA synthetase 3. *J Lipid Res*. 2018;59:805-819.
41. Li T, Lu D, Yao C, et al. Kansl1 haploinsufficiency impairs autophagosome-lysosome fusion and links autophagic dysfunction with Koolen-de Vries syndrome in mice. *Nat Commun*. 2022;13:931.
42. Nah J, Miyamoto S, Sadoshima J. Mitophagy as a protective mechanism against myocardial stress. *Compr Physiol*. 2017;7:1407-1424.
43. Dorn GW 2nd. Gone fission...: diverse consequences of cardiac Drp1 deficiency. *Circ Res*. 2015;116:225-228.
44. Tong M, Zablocki D, Sadoshima J. The role of Drp1 in mitophagy and cell death in the heart. *J Mol Cell Cardiol*. 2020;142:138-145.
45. Kleele T, Rey T, Winter J, et al. Distinct fission signatures predict mitochondrial degradation or biogenesis. *Nature*. 2021;593:435-439.
46. Kageyama Y, Hoshijima M, Seo K, et al. Parkin-independent mitophagy requires Drp1 and maintains the integrity of mammalian heart and brain. *EMBO J*. 2014;33:2798-2813.
47. Song M, Dorn GW 2nd. Mitoconfusion: non-canonical functioning of dynamism factors in static mitochondria of the heart. *Cell Metab*. 2015;21:195-205.
48. Chen M, Chen Z, Wang Y, et al. Mitophagy receptor FUNDC1 regulates mitochondrial dynamics and mitophagy. *Autophagy*. 2016;12:689-702.
49. Lee Y, Lee HY, Hanna RA, Gustafsson AB. Mitochondrial autophagy by Bnip3 involves Drp1-mediated mitochondrial fission and recruitment of Parkin in cardiac myocytes. *Am J Physiol Heart Circ Physiol*. 2011;301:H1924-H1931.
50. Cho HM, Ryu JR, Jo Y, et al. Drp1-Zip1 interaction regulates mitochondrial quality surveillance system. *Mol Cell*. 2019;73:364-376.e8.
51. Disatnik MH, Ferreira JC, Campos JC, et al. Acute inhibition of excessive mitochondrial fission after myocardial infarction prevents long-term cardiac dysfunction. *J Am Heart Assoc*. 2013;2:e000461.
52. Sharp WW, Fang YH, Han M, et al. Dynamin-related protein 1 (Drp1)-mediated diastolic dysfunction in myocardial ischemia-reperfusion injury: therapeutic benefits of Drp1 inhibition to reduce mitochondrial fission. *FASEB J*. 2014;28:316-326.

---

**KEY WORDS** CDK1, DRP1, MAMs, mitophagy, pressure overload-induced heart failure, STX17

---

**APPENDIX** For a supplemental table and figures, please see the online version of this paper.